4-2005

3D Simulation of Layer Mixing in a Three-Layer Stratified Headbox

Jatetana Kunsriluksakul

3D SIMULATION OF LAYER MIXING IN A THREE-LAYER STRATIFIED HEADBOX

by

Jatetana Kunsriluksakul

A Thesis
Submitted to the
Faculty of The Graduate College
in partial fulfillment of the
requirements for the
Degree of Master of Science
Department of Paper Engineering, Chemical Engineering and Imaging

Western Michigan University
Kalamazoo, Michigan
April 2005

ACKNOWLEDGMENTS

This thesis has been conducted in partial fulfillment of the requirements for the degree of master science Paper and Imaging Science and Engineering. The author would like to thank Dr. Dewei Qi, Dr. Paul D. Fleming, and Dr. David Peterson for their help in completing this thesis.

Jatetana Kunsriluksakul

3D SIMULATION OF LAYER MIXING IN A THREE-LAYER STRATIFIED HEADBOX

Jatetana Kunsriluksakul, M.S.

Western Michigan University, 2005

In this research, the commercially available software called FLUENT is used to simulate and visualize behaviors of flow in a three-layer stratified headbox of a paper machine. A two-phase model, "volume of fluid", is employed to simulate turbulences in a free jet. The information obtained from the simulations, in terms of velocity profiles, Reynolds stress, turbulent kinetic energy, and macro scale of turbulence, are used to assess and characterize the effect of free jet length, vane length, vane thickness, nozzle angle, and slice opening on fiber layer mixing. Importantly, the simulation results demonstrated that the macro scale of turbulence in the free jet is a critical parameter to evaluate and optimize the degree of fiber layer mixing and forming. In addition, air entrainment was observed in the three dimensional simulations. It is expected that the vane and free jet lengths are the keys of layer mixing in stratified headbox. In addition, it is better for both vane and free jet lengths to be adjustable during operation.

TABLE OF CONTENTS

ACKNOWLEDGMENTS ii

LIST OF TABLES iv

LIST OF FIGURES v

CHAPTER

I. INTRODUCTION 1

II. LITERATURE REVIEW 3

III. STATEMENT OF THE PROBLEMS AND OBJECTIVE 7

IV. EXPERIMENTAL SETUP AND METHODOLOGY 8

Simulation Methodology 8

Experimental Setup 13

V. RESULT AND DISCUSSION 20

Free Jet Length Case 20

Vane Length Case 25

Jet Speed Difference Case 30

Vane Thickness Case 36

Headbox Angle Case 42

Slice Opening Case 48

Three-dimensional Simulation of Stratified Headbox 56

VI. CONCLUSION 60

REFERENCES 61

LIST OF TABLES

1. The Summation of SFH Models in Free Jet Length Case 15
2. The Summation of SFH Models in Vane Length Case 15
3. The Summation of SFH Models in Jet Speed Difference Case 16
4. The Summation of SFH Models in Vane Thickness Case 17
5. The Summation of SFH Models in Headbox Angle Case 17
6. The Summation of SFH Models in Slice Opening Case 18
7. The Summation of SFH Model in Three-dimensional Simulation 19

LIST OF FIGURES

1. The Basic Geometrical Dimensions of SFH Models 14
2. Headbox Models of Free Jet Length Case..... 20
3. Density Contour (kg/m^3) of Free Jet Length Case 22
4. Velocity Contour (m/s) of Free Jet Length Case..... 23
5. Reynold Stress (Pascal) of Free Jet Length Case 24
6. Macro Scale of Turbulence (m) of Free Jet Length Case..... 24
7. Headbox Models of Vane Length Case..... 26
8. Relative Velocity Profile of Vane Length Case 27
9. Reynold Stress (Pascal) of Vane Length Case 28
10. Turbulent Kinetic Energy (m^2/s^2) of Vane Length Case..... 28
11. Macro Scale of Turbulence (m) of Vane Length Case..... 29
12. Velocity Contour (m/s) of Different Jet Speed Case..... 31
13. Turbulent Intensity Contour (%) of Different Jet Speed Case 32
14. Energy Dissipation (m^2/s^3) Contour of Different Jet Speed Case in Logarithmic Scale..... 33
15. Relative Velocity Profile of Different Jet Speed Case..... 34
16. Reynolds Stress (Pascal) of Different Jet Speed Case..... 35
17. Turbulent Kinetic Energy (m^2/s^2) of Different Jet Speed Case..... 36
18. Macro Scale of Turbulence (m) of Different Jet Speed Case..... 36
19. Headbox Models of Vane Thickness Case..... 37
20. Contour of Turbulent Intensity (%) of Vane Thickness Case 38

List of Figures—continued

21. Energy Dissipation (m^2/s^3) Contour of Different Jet Speed Case in Logarithmic Scale 39

22. Relative Velocity Profile of Vane Thickness Case 40

23. Reynolds Stress (Pascal) of Vane Thickness Case 41

24. Turbulent Kinetic Energy (m^2/s^2) of Vane Thickness Case 41

25. Macro Scale of Turbulence (m) of Vane Thickness Case 42

26. Headbox Models of Headbox Angle Case 43

27. Relative Velocity Profile of Headbox Angle Case 45

28. Reynolds Stress (Pascal) of Headbox Angle Case 47

29. Turbulent Kinetic Energy (m^2/s^2) of Headbox Angle Case 47

30. Macro Scale of Turbulence (m) of Headbox Angle Case 48

31. Headbox Models of Slice Opening Case 49

32. Contour of Turbulent Intensity (%) of Slice Opening Case 50

33. Energy Dissipation (m^3/s^2) Contour of Slice Opening Case in Logarithmic Scale 52

34. Relative Velocity Profile of Slice Opening Case 53

35. Reynolds Stress (Pascal) of Slice Opening Case 55

36. Turbulent Kinetic Energy (m^2/s^2) of Slice Opening Case 55

37. Macro Scale of Turbulence (m) of Slice Opening Case 56

38. 3D Geometry of Headbox and Free Jet in 3D Case 57

39. Headbox Models of Headbox in 3D Case 57

40. Plot of Volume Fraction of Water at The Wake Area Behind The Vane 58

41. Density Contour (kg/m^3) on CD direction at the Plane between the Top Layer and Center Layer 59

CHAPTER I

INTRODUCTION

Manufacturers of printing/writing paper and linerboard have long been interested in placing fibers in different layers to form multi-layered sheets [1-6]. This multi-layered technique takes an advantage of different fiber properties to produce a higher quality sheet [7]. With this technique, it is possible to place a lower grade of fibers at the middle layer and use printing surface quality fibers for the printing surface. This technique is not only successful in the low basis weight tissue grades, but also in the high basis weight packaging grades [3-4,8].

Historically, multi-layer board originated from cylinder formers and multi-fourdrinier formers in 1960. There are two objectives of multi-layer web forming: quality improvement and fiber economy. For layered tissue grades, the objective of multi-layer forming is to improve quality by using the high-grade fibers on surface layers to achieve a bright, soft and smooth outer surface. In the case of linerboard, the objective is to reduce cost by placing lower grade fibers in the center and the virgin fiber on the outside layers to maintain better surface appearance and mechanical properties. For printing and writing grades, multi-layer forming is used to place the shorter fibers and fillers on the surface for smoothness, bulk and printability, while the stronger fibers in the center of the sheet for good mechanical properties. [3,7]

The multi-layered or multi-ply sheet has been a success in both the board and tissue industries by using a separate headbox and forming wire for each layer on a Fourdrinier machine. However, this method may result in a high investment cost on mechanical and controlling equipment and increases the maintenance cost, such as

spare parts, rolls and wires, and the high production time loss when it is shutdown for maintenance. Therefore, a stratified forming headbox has been developed in order to duplicate the effectiveness of separate headboxes. The most important aspect in the development of stratified forming is capable of combining multiple stock flows into one jet or simultaneously forming the multi-layer sheet with a single headbox. By using separate vanes, each layer is separated inside the headbox, and each layer is mixed with other layers at the outlet. Because of the simultaneous forming, the stratified headbox with less equipment is believed to be more economic with a less investment cost and a lower energy consumption [2,7-9].

Currently, this technology has been used in the tissue industry. It is particularly applicable with twin-wire/gap former, because the forming is going to set the sheet quickly [8]. However, only a very small number of printing/writing paper and paperboard mills have even tried this technology. The sheet quality is not easy to control in this type of headbox. Fiber migration between layers causes the heterogeneous surface with an uneven formation, which worsens the printability. Nevertheless, stratified forming technology may play an increased role in the future of papermaking if the key operating problems have been resolved [8].

Nowadays, computer simulation methods have become an efficient tool, simulating the interactions of fluids. High accuracy and low cost makes this simulation technique very attractive. As there are many factors affecting layer mixing in a stratified headbox, it is very expensive to study all of them by experiment. Therefore, the simulation technique is employed to investigate the layer mixing phenomena in a stratified headbox. These simulation results would be used as guidelines for further designing a pilot stratified headbox.

CHAPTER II

LITERATURE REVIEW

The disadvantage of a Stratified Forming Headbox (SFH) is that the lower grade fibers at the center (inner) layer migrate to the paper surface, resulting in heterogeneous surface, poor paper formation and inferior printability.

Typically, a SFH is a converging channel in which elastic vanes are pinned at one end and are free to move at the other end. The position of vanes inside a headbox depends on their bending stiffness and the forces generated by fluid flow. Fibers from different layers are separated by vanes and then mixed together after the vanes end. There are many factors affected layer mixing, such as vane length, vane thickness, slice opening and headbox angle. Following is a review of previous studies on each factor.

Lloyd and Norman [10] and Li, Neill and Rogers [11-12] studied the role of vane length on a three-layer stratified forming headbox. They found that vanes shorter than the length of the headbox nozzle led to low turbulence intensity, while longer vanes led to more intense turbulence from a narrower channel. The turbulence scale of shorter vanes was too large and their intensity is too small to break down the fiber flocs; instead, this low intensity turbulence only mixed all fibers together causing a heterogeneous surface, which worsens the printability. Higher flow rate in a narrower channel with the longer vanes produces more intense turbulence and a smaller scale of turbulence, which can break down the flocs and make the surface more homogenous and uniform. Nevertheless, very long vanes caused complete turbulent mixing of the different layers that result in very poor sheet formation and printability.

The effect of slice lip was also studied by Lloyd and Norman [13]. The shape of slice lips was evaluated by comparing a parrot's beak slice lip with converging and parallel slice lips. They found that the type of slice lip did not affect the layer mixing when the vane length is longer than the nozzle. The Parrot's beak slice lip increased the scale of turbulence and led to increase in the layer mixing, because it gave a wider channel at the vane tips, allowing the turbulence to grow to a larger scale.

The effect of slice opening and different jet speeds were also studied by Llyod and Norman [13] and Li, Neill and Rogers [11-12]. Lloyd and Norman [13] found that the narrower slice opening led to lower layer mixing. This result was completely different from that by Li, Neill and Rogers [11-12]. However, their similar result is that the different jet speeds have no significant influence on the layer mixing of SFH.

A Stepped vane is typically used in a headbox to increase floc-breaking turbulence. The effect of the step extension in SFH was studied by Lloyd and Norman [14]. They concluded that stepped vanes are not the answer to reduce the layer mixing in SFH.

The layer mixing mainly occurs at the free jet area between the headbox outlet and wire former. The mixing characteristics of three-layer SFH on this free jet was studied by Li, Neill and Rogers [11-12]. They studied by using fresh water in the top and bottom layers, while using the salt water in the center layer to create a marked difference in the conductivity level. The conductivity data at difference locations on the free jet (the distance between headbox jet outlet and wire forming), were used to determine the layer mixing in terms of the relative changes in the conductivity profile. They found that the free jet tends to promote the transport of the salt solution from the center layer to the top and bottom layers. As the free jet length increases, the conductivity of the jet surface continually increases. They also found that the jet

speed difference has no significant influence on the layer mixing intensity, that is the same as the experiment by Lloyd and Norman [13]. Importantly, Li, Neill and Rogers [11,12] found that the variation of free jet length causes different degrees of layer mixing. For the long free jet length, the shortest vane gives the lowest layer mixing. On the other hand, the longest vane produces the least layer mixing for the short free jet length. They suggested that the free jet length has a strong influence on the optimum choice of the length of the vane. [11-12]

Numerical simulation of a SFH was carried out by Parsheh and Dahlkild [4]. The effect of vane length, vane shape and slice opening was similar to the experiment by Lloyd and Norman [10,13-14]. In addition, they studied the effect of vane thickness and headbox angle on layer mixing. They concluded that the layer mixing is mostly affected by the turbulence between adjacent layers when they exit the headbox, by the boundary layer thickness at the headbox outlet and by the wake area behind the vane. Importantly, they suggested that the optimum headbox angle should be around 8 to 11 degrees in order to give the lowest layer mixing. [4]

Another computational fluid simulation on SFH was done by Farrington [15]. His simulation was done on three types of Tissue machine headboxes. He theoretically explained that formation and disruption of fiber flocs are dynamic processes, which depend on the level of turbulent stresses, time of exposure to these stresses, fiber characteristics and concentration. Many literature data suggested that Reynolds stresses in the 10-100 Pa range are required depending on fiber species and concentration to disrupt the fiber flocculation. Farrington also determined the size of fiber flocs by estimating from the scale of turbulence and turbulent kinetic energy. Since large flocs must be avoided, a headbox must generate high turbulent kinetic energy and fine scale turbulence to prevent fiber flocculation. The uniformity of flow

velocity at the headbox exit is required to make better sheet formation. The velocity profile should be uniform across the nozzle exit and free from any wake effects. He found that the parallel channel produce a more fully developed turbulent flow than the converging channel. Wakes decay most rapidly in the parallel channel, giving a more uniform exit velocity profile. The increasing slice opening at constant jet exit velocity increases the turbulent in the larger region as the result in the increasing macro scale of turbulence. This result is similar to the experiment by Lloyd and Norman [13]. He concluded that the converging channel headbox produces the finest scale of turbulence and the lowest fiber flocculation. [15]

The free jet has never been studied and optimized by fluid dynamic simulation techniques. The turbulence in terms of scale and intensity has never been properly used to explain the layer mixing in SFH. In this research, a two-phase model, called volume of fluid, is employed in the simulations of free jet. The simulation results, in terms of velocity profiles, turbulent kinetic energy, and macro scale of turbulence, are used to assess and characterize the effect of free jet length, vane length, vane thickness, jet speed different, nozzle angle, and slice opening on fiber layer mixing.

CHAPTER III

STATEMENT OF THE PROBLEMS AND OBJECTIVE

The major problem of a stratified headbox is that the lower grade fibers at the center (inner) layer migrate to the paper surface causing poor formation and inferior printability. At the present, many factors such as vane length, vane shape, vane thickness, free jet area and slice opening, will affect the layer mixing. Due to the high cost of pilot machines, the low cost of simulation techniques is applied to study all factors affected the layer mixing of SFH.

The aim of this research is to characterize and visualize the effect of free jet length, vane length, vane thickness, nozzle angle, and slice opening on fiber layer mixing in SFH. This simulation results will be discussed and compared with the previous experiments in order to find the way to reduce the layer mixing. It is expected that the result will facilitate the design of a SFH that has the optimum turbulent level to break up fiber flocculation and the small scale of turbulence to prevent fibers from the inner layer migrating to the paper surface.

CHAPTER IV

EXPERIMENTAL SETUP AND METHODOLOGY

Simulation Methodology

The commercial computational fluid simulation program used in this research is FLUENT version 5.5. The models of stratified headbox are created by using GAMBIT program version 2.0. The computational details used in this research are shown as follow:

Turbulence Model

Generally, the fibers inside the headbox are in a very low consistency of 0.5 – 1.0% slurry. Only water will be used in this simulation and the results would not be significantly different from those that include fibers [15-16].

As the fluid in a headbox is incompressible, FLUENT solves conservation equations given by equations, (1) and (2), for mass and momentum, respectively. [15,17-18]

$$\frac{\partial}{\partial x_i}(\rho u_i) = 0 \tag{1}$$

$$\frac{\partial}{\partial x_i}(\rho u_i u_j) = \frac{\partial}{\partial x_i}(\mu\left[\frac{\partial u_i}{\partial x_j} + \frac{\partial u_j}{\partial x_i}\right]) - \frac{\partial p}{\partial x_j} + \frac{\partial}{\partial x_i}(\overline{\rho u'_i u'_j}) \tag{2}$$

where ρ is the density of fluid (kg/m^3)

u_i is velocity components (m/s)

u'_i is fluctuating velocities components (Pascal)

μ is dynamic viscosity (Pa-s)

x_i is Cartesian coordinate (m)

The standard $k-\varepsilon$ model is employed to calculate the turbulence. The equations and the standard parameters are given by equation (3) to (8) [15, 17].

$$\overline{\rho u'_i u'_j} = \rho(2/3)k\delta_{ij} + \mu_t(\frac{\partial u_i}{\partial x_j} + \frac{\partial u_j}{\partial x_i}) \tag{3}$$

where k is turbulent kinetic energy (m^2/s^2)

μ_t is turbulent viscosity (Pa-s)

δ_{ij} is equal to 1 if $i = j$.

$$\frac{\partial}{\partial x_i}(\rho u_i k) = \frac{\partial}{\partial x_i}(\frac{\mu}{\sigma_k}\frac{\partial k}{\partial x_i}) + G_k - \rho\varepsilon \tag{4}$$

where ε is turbulent energy dissipation (m^2/s^3).

$$\frac{\partial}{\partial x_i}(\rho u_i \varepsilon) = \frac{\partial}{\partial x_i}(\frac{\mu}{\sigma_\varepsilon}\frac{\partial \varepsilon}{\partial x_i}) + C_1\frac{\varepsilon}{k}G_k - C_2\rho\frac{\varepsilon^2}{k} \tag{5}$$

$$G_k = \mu_t(\frac{\partial u_i}{\partial x_j} + \frac{\partial u_j}{\partial x_i})\frac{\partial u_i}{\partial x_j} \tag{6}$$

$$\mu_t = \rho C_\mu \frac{k^2}{\varepsilon} \tag{7}$$

$$C_1 = 1.44, C_2 = 1.92, C_\mu = 0.09, \sigma_k = 1.0, \sigma_\varepsilon = 1.3 \tag{8}$$

The model constants on equation (8) have been determined from experiments with air and water for fundamental turbulent shear flows by FLUENT. It has been found that the model constants work very well for a wide range of wall-bounded and free shear flows. [17]

Two-phase fluid model

The Volume of Fluid (VOF) model is the most suitable computation model to include the interface between air and water. The VOF model is a fixed grid technique designed for two or more immiscible fluids where the position of the interface between the fluids is of interest. In the VOF model, a single set of momentum

equations is shared by the fluids, and the volume fraction of each of the fluids in each computational cell is tracked throughout the domain. [19-21]

The VOF model relies on the fact that two or more fluids are not interpenetrating. For each additional phase, a variable, its volume fraction, is introduced in the computational cell. In each control volume, the volume fractions of all phases are summed to unity. The fields and properties are shared by the phases. Thus the variables and properties are either purely representative for one of the phases, or for a mixture of the phases, depending upon the volume fraction values. In other words, if the q^{th} fluid's volume fraction is denoted as α_q, then the following three conditions are possible: [19]

$\alpha_q = 0$ the cell is empty of the q^{th} fluid.

$\alpha_q = 1$ the cell is full of the q^{th} fluid.

$0 < \alpha_q < 1$ the cell contains the interface between the fluids.

The tracking of the interfaces between the phases is accomplished by the solution of a continuity equation for the volume fraction of one or more of the phases. For the q^{th} phase, the volume fraction equation has the following form: [19]

$$\frac{\partial \alpha_q}{\partial t} + u_i \frac{\partial \alpha_q}{\partial x_i} = 0 \tag{9}$$

The properties appearing in the transport equations are determined by the presence of the component phases in each control volume. For the q^{th} phase, the volume-fraction-averaged density takes on the following form: [19]

$$\rho = \Sigma \alpha_q \rho_q \tag{10}$$

In addition, other properties, such as viscosity, are computed in this manner. Therefore, the momentum equation, in equation (2), is dependent on the volume fractions of all phases through ρ and μ properties. [19]

Surface Tension

The effect of the surface tension is included in this simulation. In FLUENT, the addition of surface tension to VOF calculation results in a source term in the momentum equation. A formulation of the surface tension force is computed from the gradients in the surface normal at the interface. The surface normal (n), defined as the gradient of α_q is calculated by equation (11).

$$n = \nabla \alpha_q \tag{11}$$

where n is the surface normal at the interface

The curvature (κ) is defined in terms of the divergence of the unit normal ($\hat{n}$) as calculated by equation (12). The unit normal ($\hat{n}$) is calculated by equation (13).

$$\kappa = \nabla \cdot \hat{n} \tag{12}$$

$$\hat{n} = \frac{n}{|n|} \tag{13}$$

The surface tension can be written in terms of the pressure jump across the surface. The force at the surface can be expressed as a volume force using the divergence theorem as shown in equation (14).

$$F_{vol} = \sum_{pairsij, i<j} \sigma_{ij} \frac{\alpha_i \rho_i \kappa_j \nabla \alpha_j + \alpha_j \rho_j \kappa_i \nabla \alpha_i}{\frac{1}{2}(\rho_i + \rho_j)} \tag{14}$$

This volume force from the surface tension effect (F_{vol}) is added to the momentum equation as in the equation (2).

Initial and Boundary Conditions

In this simulation, the target of the jet velocity outlet is around 15 – 20 m/s, which is approximated to 900 – 1,200 m/min. Therefore, the velocity inlet of each layer is set and adjusted until the jet velocity outlet is in the target range.

It is suggested by FLUENT [17,22] that 5 ~ 10 % of the inlet turbulent

intensities (I) is enough to represent the fully-developed turbulence. Since the turbulent eddies cannot be larger than the duct, turbulent length scale (l) is approximate from the physical size of channel by $l = 0.07 * L$, where L is the size of channel and the factor of 0.07 is based on the maximum value of the mixing length in fully-developed turbulent pipe flows [22]. Therefore, the turbulent kinetic energy (k_0) and the energy dissipation (ε_0) are then calculated from the turbulent intensity (I) and turbulent length scale (l) by equation (11) and (12) [15,17,22].

$$k_0 = \frac{3}{2}(V_{in} * I)^2 \tag{11}$$

$$\varepsilon_0 = C_\mu^{\frac{3}{4}}\left(\frac{k_0^{3/2}}{l}\right) \tag{12}$$

where V_{in} is the velocity inlet of fluid (m/s)

C_1 is the constant of turbulent model as shown in equation (8)

Performance Criteria

In general, the turbulence inside the headbox is required to break up the flocs in each layer. Farrington Jr. [15] used the magnitude of total Reynolds stresses (R) to investigate the flocs disruption inside the headbox channel, which is estimated from equation (13) and (14). Therefore, Reynolds stresses (R) and turbulent kinetic energy (k) could be used to evaluate the turbulent level or shear stress broken up flocs in each layers. [15]

$$-R_{ij} = \left(\frac{\mu_t}{\rho}\right)\left(\frac{\partial u_i}{\partial x_j} + \frac{\partial u_j}{\partial x_i}\right) - \left(\frac{2}{3}\right)\delta_{ij}k \tag{13}$$

$$|R| = \Sigma|R_{ij}| : i \geq j \tag{14}$$

$$\lambda = k^{3/2}/\varepsilon \tag{15}$$

Importantly, the macro scale of turbulence (λ) in equation (15) is defined as the integral length scale. The macro scale may represent the scale at which turbulent

quantities remain self-correlated or the scale of energy-containing eddies [20]. In the other word, it refers to the size of the large eddies that contain the energy in turbulent flows [21] or the range of scales for fluctuating velocities [22]. Therefore, this macroscopic scale of turbulence (λ) at the interface area between the top (or bottom) surface layer and the center (inner) layer will be used to characterize the floc size [15] and the layer mixing level.

In addition, the flow uniformity is desirable for jet-wire forming. Therefore, four performance parameters, magnitude of total Reynolds stress, macro scale of turbulence (λ), turbulent kinetic energy (k), and jet outlet velocity profile, are used to asses the levels of layer mixing in SFH. The results will be compared with the previous experiments.

Experimental Setup

The Basic Shape of SFH Model

In order to make the simulation results more reliable and comparable to the previous studies, the design of three-layer stratified headbox in this study is based on the pilot stratified headbox used by Lloyd and Norman [10,13-14]. The basic geometrical dimension of headbox used in this research is shown in Figure 1.

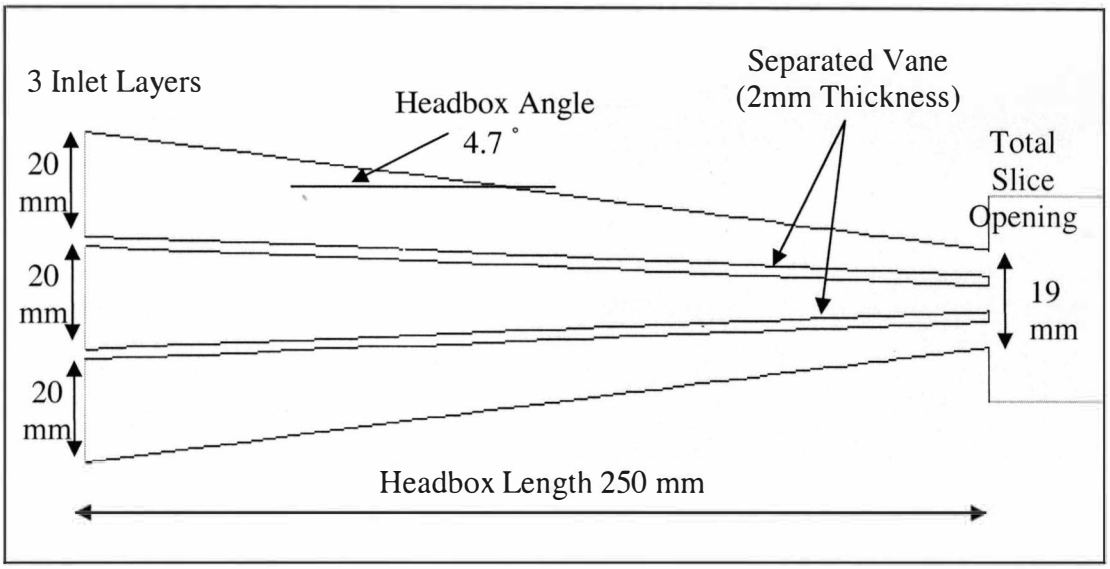

Figure 1. The Basic Geometrical Dimensions of SFH Models.

Studied Factors Affect Layer Mixing

The seven factors studied in this research are free jet length, vane length, jet speed difference, vane thickness, headbox angle, slice opening and the effect on Cross-machine Direction (CD). The experiment setup for each factor is showed as follow:

Free Jet Length

The free jet length is the distance from the headbox outlet to the forming wire. The free jet in this work is the interface area between air and water. A two-phase model, called Volume of Fluid (VOF), is employed to simulate the turbulence in this area. In order to prove that this two-phase model is working properly, the two different free jet lengths, 300 mm and 500 mm, are simulated in this case. The summation of headbox models is shown in Table 1.

Table 1

The Summation of SFH Models in Free Jet Length Case

Relative Vane Length (mm)	Inlet Size (mm)	Headbox Angle (degree)	Vane Thick-ness (mm)	Total Slice Opening (mm)	Free Jet Length (mm)	Total Model Length (mm)	Inlet Vel (m/s)
+0	20	4.7	2	19	300	550	5
+0	20	4.7	2	19	500	750	5

Vane Length

The relative vane length (RVL) is defined as a subtraction of the vane length from the headbox length (250mm). For example, the case with RVL +0 mm is that the vane length is equal to the headbox length as shown in Figure 1. At the present, it was found that the vane length played a significant role on the layer mixing. Therefore, three cases with RVL= -50, 0, +50 mm are simulated to investigate the layer mixing on the free jet in this case. The summation of SFH models with three different RVL is shown in Table 2.

Table 2

The Summation of SFH Models in Vane Length Case

Relative Vane Length (mm)	Inlet Size (mm)	Headbox Angle (degree)	Vane Thick-ness (mm)	Total Slice Opening (mm)	Free Jet Length (mm)	Inlet Vel (m/s)
-50	20	4.7	2	19	500	5
+0	20	4.7	2	19	500	5
+50	20	4.7	2	19	500	5

Jet Speed Difference

Generally, the turbulence intensity inside the headbox is proportional to the jet speed or fluid velocity. For that reason, the different jet speeds are expected to affect the layer mixing. As the jet speed is adjusted by the inlet velocity of each layer, three different jet speeds simulated are 5, 10 and 15 m/s of the inlet velocity of each layer. The summation of SFH models in this case is shown in Table 3.

Table 3

The Summation of SFH Models in Jet Speed Difference Case

Relative Vane Length (mm)	Inlet Size (mm)	Headbox Angle (degree)	Vane Thick-ness (mm)	Total Slice Opening (mm)	Free Jet Length (mm)	Inlet Vel (m/s)
+0	20	4.7	2	19	500	5
+0	20	4.7	2	19	500	10
+0	20	4.7	2	19	500	15

Vane Thickness

The vane thickness varies while keeping slice opening constant at 5 mm/layer. Additional three simulations are conducted for optimization of the vane thickness. The dimensions of the headbox models with the vane thickness variation are shown in Table 4.

Table 4

The Summation of SFH Models in Vane Thickness Case

Relative Vane Length (mm)	Inlet Size (mm)	Headbox Angle (degree)	Vane Thick-ness (mm)	Total Slice Opening (mm)	Free Jet Length (mm)	Inlet Vel (m/s)
+0	20	4.9	1	17	500	5
+0	20	4.7	2	19	500	5
+0	20	4.5	3	21	500	5

Headbox Angle

The inlet width of each layer in this case varies to obtain different headbox angles, while keeping the slice opening constant. The velocity in the inlet is adjusted to have the same average jet velocity in the outlet as the inlet dimension changes. In this case, five simulations of different headbox angles are conducted for optimization of the headbox angle. The dimensions of headbox models with angle variation are shown in Table 5.

Table 5

The Summation of SFH Models in Headbox Angle Case

Relative Vane Length (mm)	Inlet Size (mm)	Headbox Angle (degree)	Vane Angle (degree)	Vane Thick-ness (mm)	Total Slice Opening (mm)	Free Jet Length (mm)	Inlet Vel (m/s)
+0	10	1.7	0.8	2	19	500	9.0
+0	13	2.8	0.9	2	19	500	7.5
+0	20	4.7	1.7	2	19	500	5.0
+0	35	10.2	3.4	2	19	500	2.7
+0	51	15.4	5.2	2	19	500	1.6

Slice Opening

Typically, the vane and headbox angles change when the slice opening varies. This effect is the normal operating condition of paper machine. Therefore, vane and headbox angles are changed as the slice opening varies in this case. The velocity in the inlet is adjusted to have the same average jet velocity in the outlet, as the channel inside the headbox changes. The headbox dimensions with different slice openings are collected in Table 6.

Table 6

The Summation of SFH Models in Slice Opening Case

Relative Vane Length (mm)	Inlet Size (mm)	Headbox Angle (degree)	Vane Angle (degree)	Vane Thick-ness (mm)	Total Slice Opening (mm)	Free Jet Length (mm)	Inlet Vel (m/s)
+0	20	5.5	1.8	2	16	500	4
+0	20	4.7	1.7	2	19	500	5
+0	20	4.3	1.4	2	26.5	500	6.5
+0	20	3.4	1.2	2	34	500	7.5

Three-dimensional Simulation of Stratified Headbox

A three-dimensional simulation is carried out to investigate the effect of layer mixing on Cross-machine Direction (CD) in the free jet. The optimized vane thickness and headbox angle will be used in this case. The details of headbox dimensions are shown in Table 7. The total width of headbox is 100 mm. Due to the symmetry assumption, only a half of the headbox and free jet is simulated. The water fluid in the free jet is surrounded by the air with 10 mm thickness.

Table 7

The Summation of SFH Models in Three-dimensional Simulation

Relative Vane Length (mm)	Inlet Size (mm)	Headbox Angle (degree)	Vane Angle (degree)	Vane Thick-ness (mm)	Total Slice Opening (mm)	Free Jet Length (mm)	Inlet Vel (m/s)
+0	20	4.7	1.7	1	19	500	5

CHAPTER V

RESULT AND DISCUSSION

Free Jet Length Case

Two cases with different jet length (300 mm and 500 mm) are simulated as shown in Figure 2. The results of the density distributions in water and air phases show the free jet slightly curved around the slice opening area due to the surface tension in figure 3.

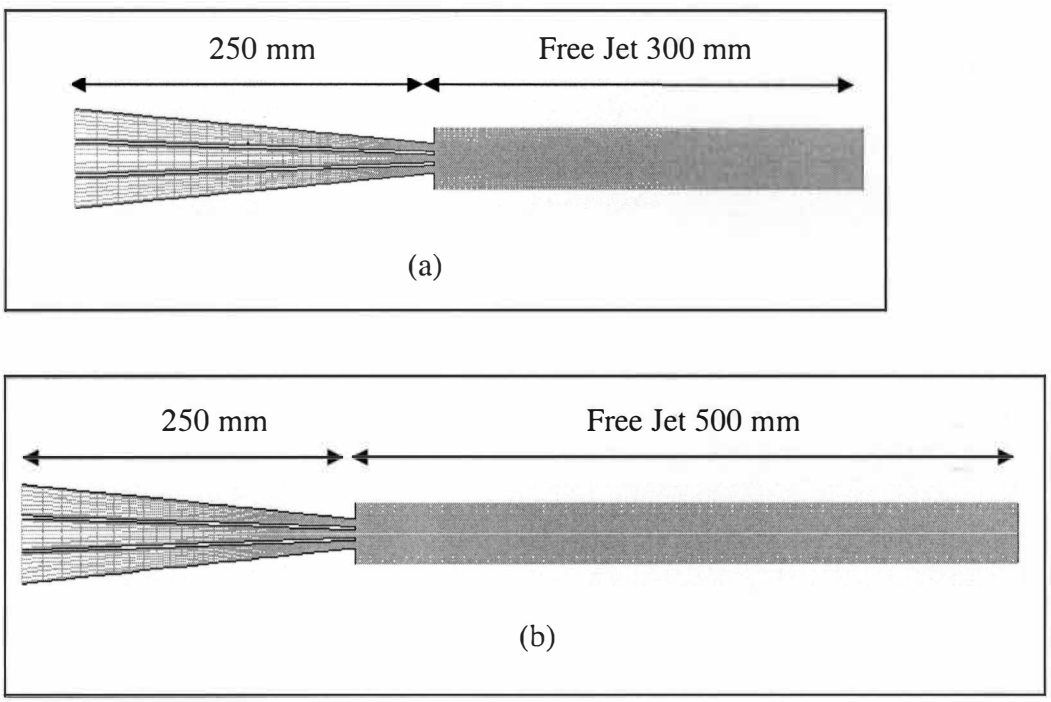

Figure 2. Headbox Models of Free Jet Length Case.
(a) Free Jet Length 300 mm.
(b) Free Jet Length 500 mm.

From Figure 3, the blue color is referred to the density of air, while the red color is referred to the density of water. Only small area between blue and red colors is where the air and water are mixed together. Figure 4 shows the velocity contour (m/s) of the jet outlet on the free jet.

The average Reynolds stress as a function of horizontal down stream position X are shown in Figure 5. The macro scale of turbulence (λ) at the jet plane between the top layer and center layer is plotted versus the horizontal down stream position X for these two cases in Figure 6. These figures show that the results of the Reynolds stress and macro scale of turbulence are the same over the range between X = 250 mm and X = 500 mm for both cases. Therefore, the variation of free jet length does not affect the simulation results.

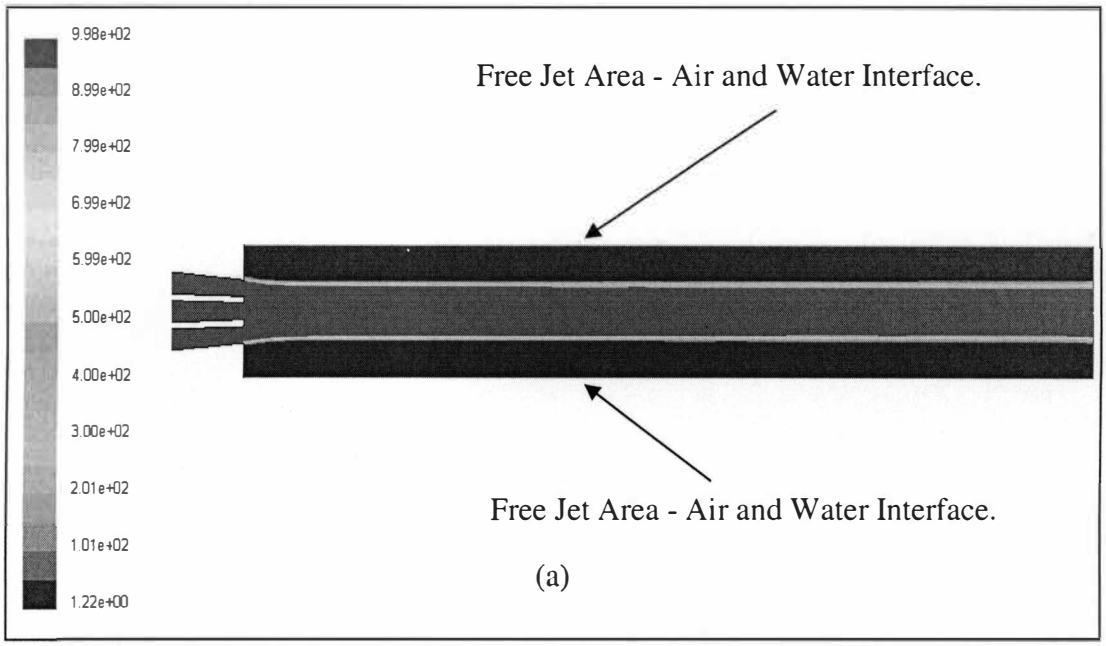

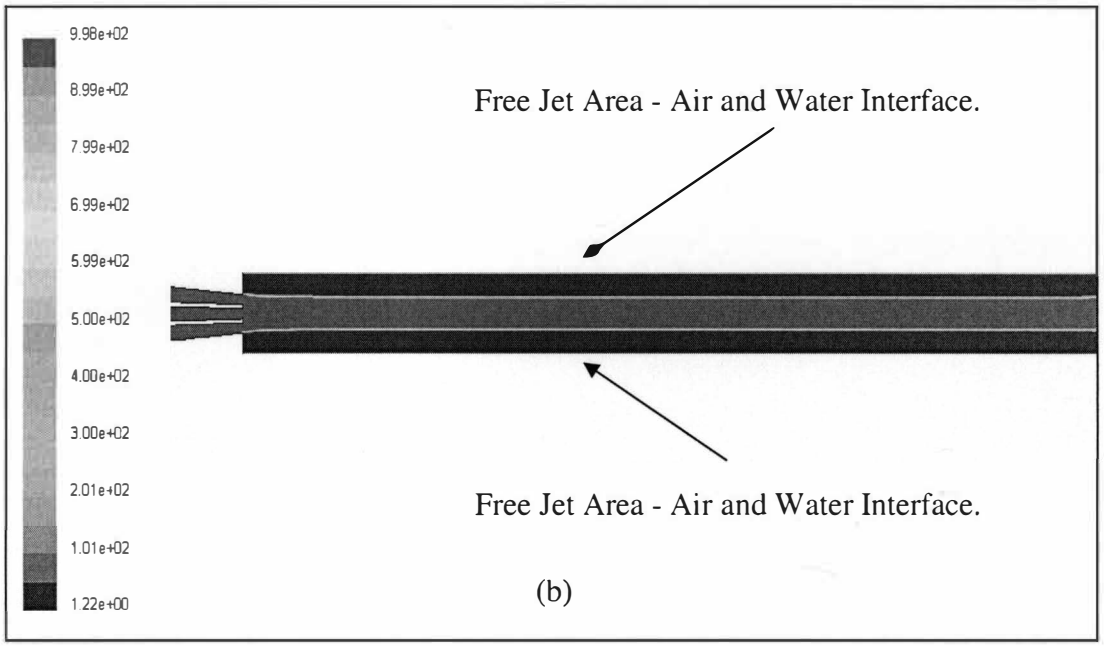

Figure 3. Density Contour (kg/m^3) of Free Jet Length Case.
(a) Free Jet Length 300 mm.
(b) Free Jet Length 500 mm.

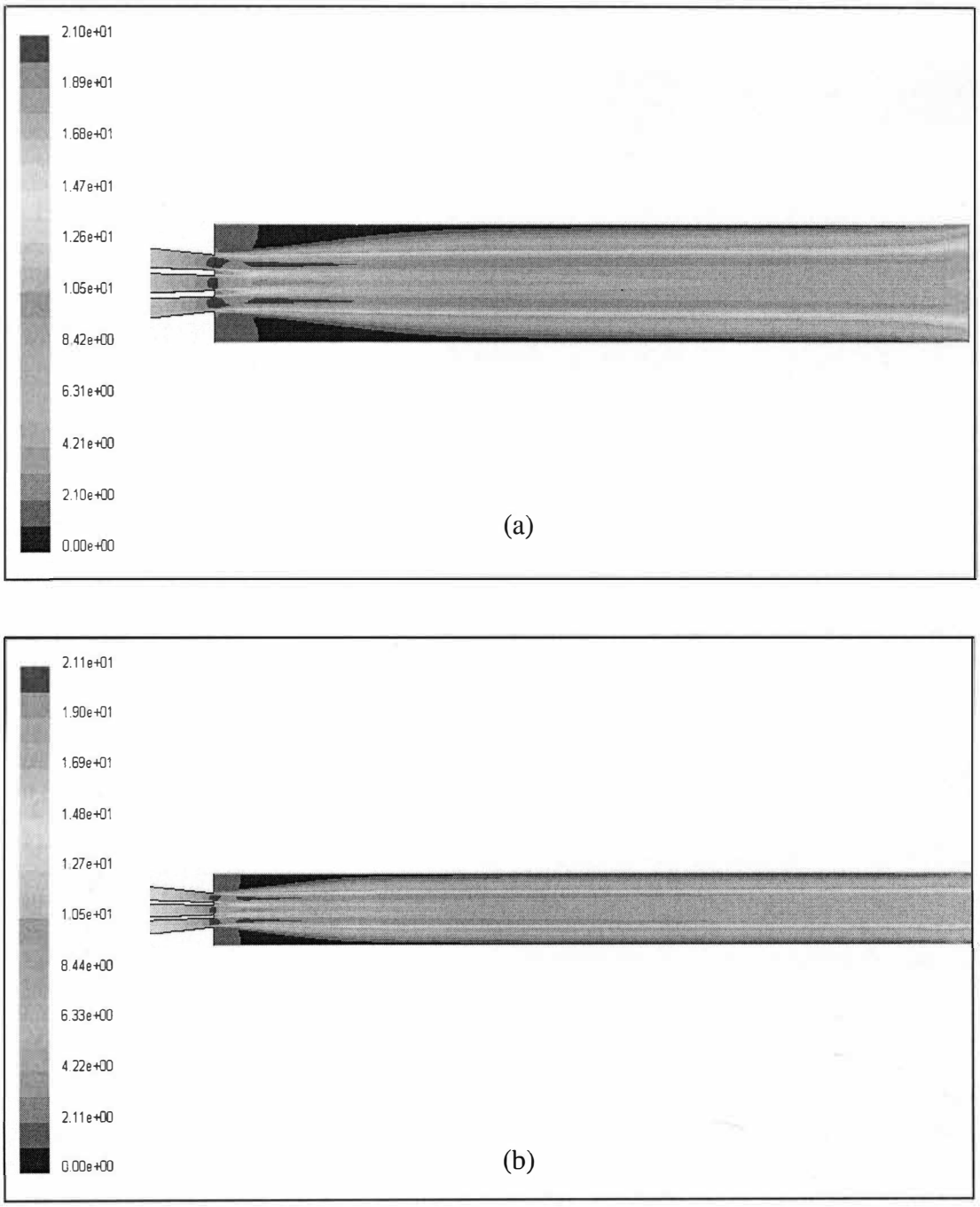

Figure 4. Velocity Contour (m/s) of Free Jet Length Case.
(a) Free Jet Length 300 mm.
(b) Free Jet Length 500 mm.

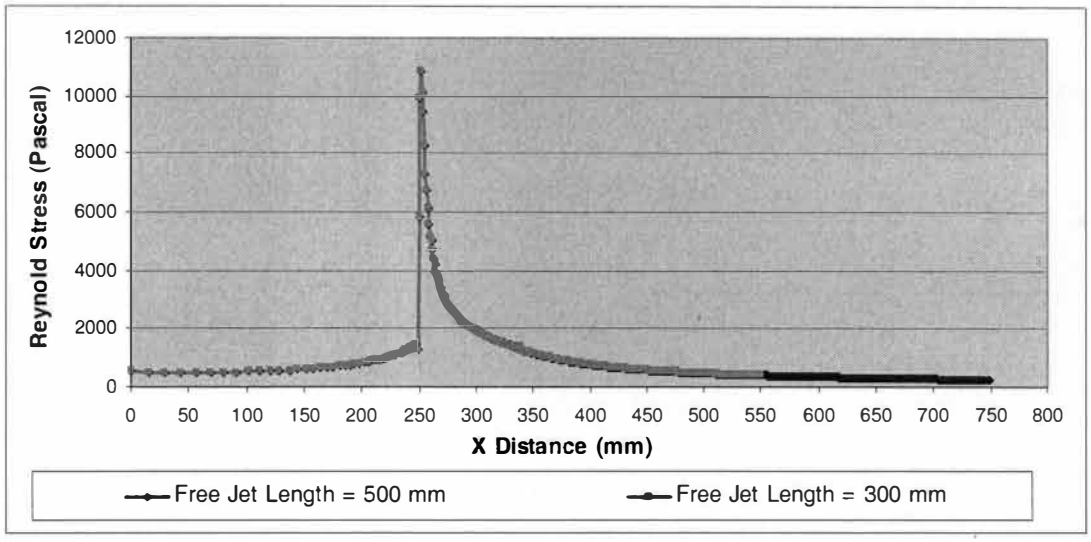

Figure 5. Reynolds Stress (Pascal) of Free Jet Length Case.

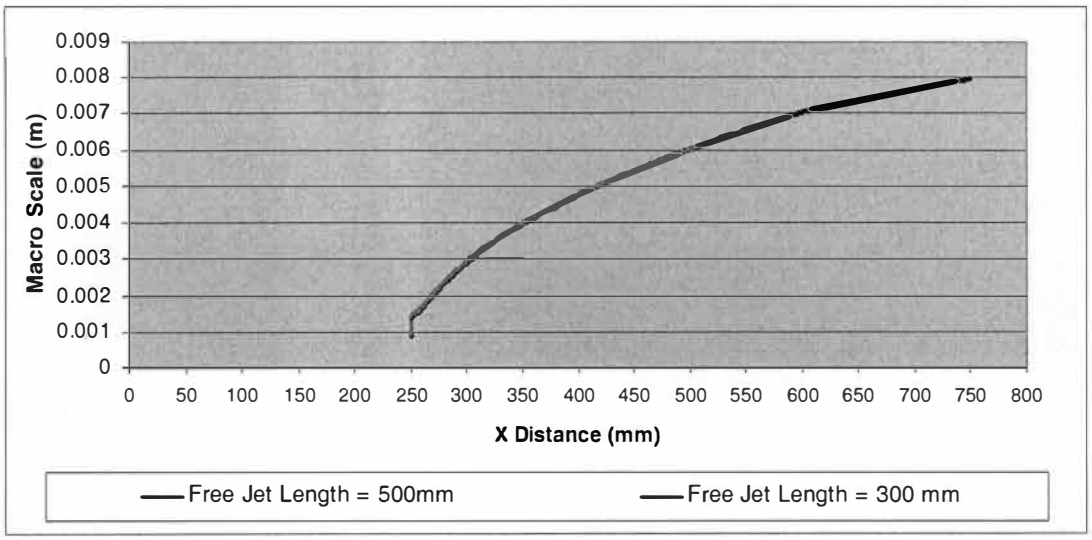

Figure 6. Macro Scale of Turbulence (m) of Free Jet Length Case.

Vane Length Case

Three SFH models with RVL= -50, 0, +50 mm are simulated in this case. These models are shown in Figure 7(a), 7(b) and 7(c), respectively.

The results of relative velocity profile for the three cases as mentioned above are plotted in Figure 8. The horizontal axis in this figure is in the thickness direction of the free jet, where zero is located at the thickness centerline of the free jet. Only the upper half area above the centerline needs to be shown due to the assumption of symmetry. In the figure, the vertical axis shows the jet velocity relative to the mean jet velocity. The velocity distribution along the jet thickness direction at a given horizontal down stream position X has the same symbol in the figure. It is clearly shown that the length of vane affects the decay of wakes produced by the vane tip. The wakes decay most rapidly in the shortest vane case (RVL= -50 mm) giving a more uniform velocity profile than the longer vane.

The average Reynolds stress and turbulent kinetic energy (k) as a function of horizontal down stream position X are shown in Figure 9 and 10, respectively. The values of the Reynolds stress and turbulent kinetic energy are referred as the level of turbulence.

The longer vane produces the higher Reynolds stress and turbulent kinetic energy (k) due to relatively narrower channel. This high turbulent shear force tends to break down the flocs in each fiber layer and gives better fiber dispersion. This simulation results are consistent with the previous experimental result [10], that is, the longest vane produces fewer flocs and the shortest vane generate the largest flocs.

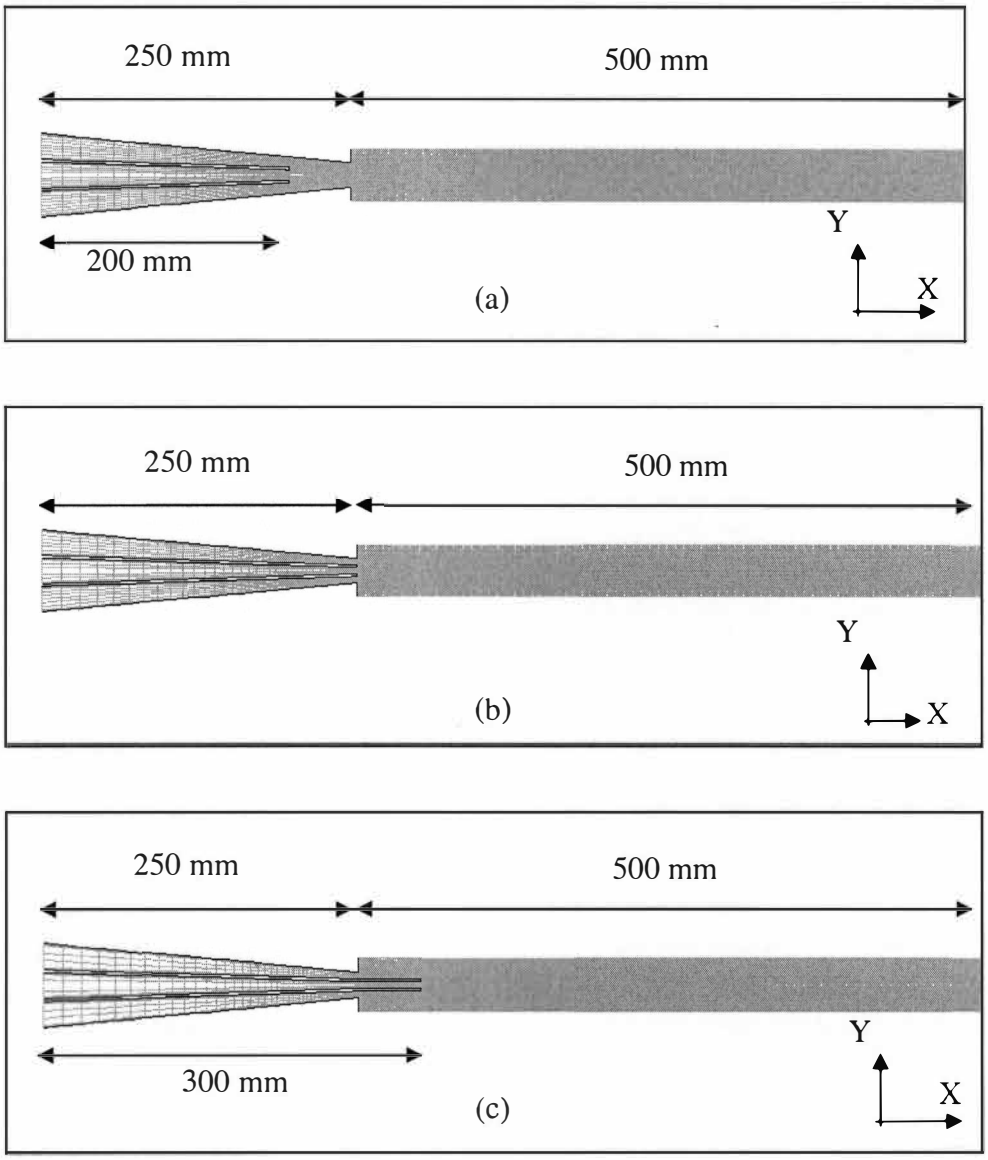

Figure 7. Headbox Models of Vane Length Case.
(a) RVL= -50 mm.
(b) RVL= +0 mm.
(c) RVL= +50 mm.

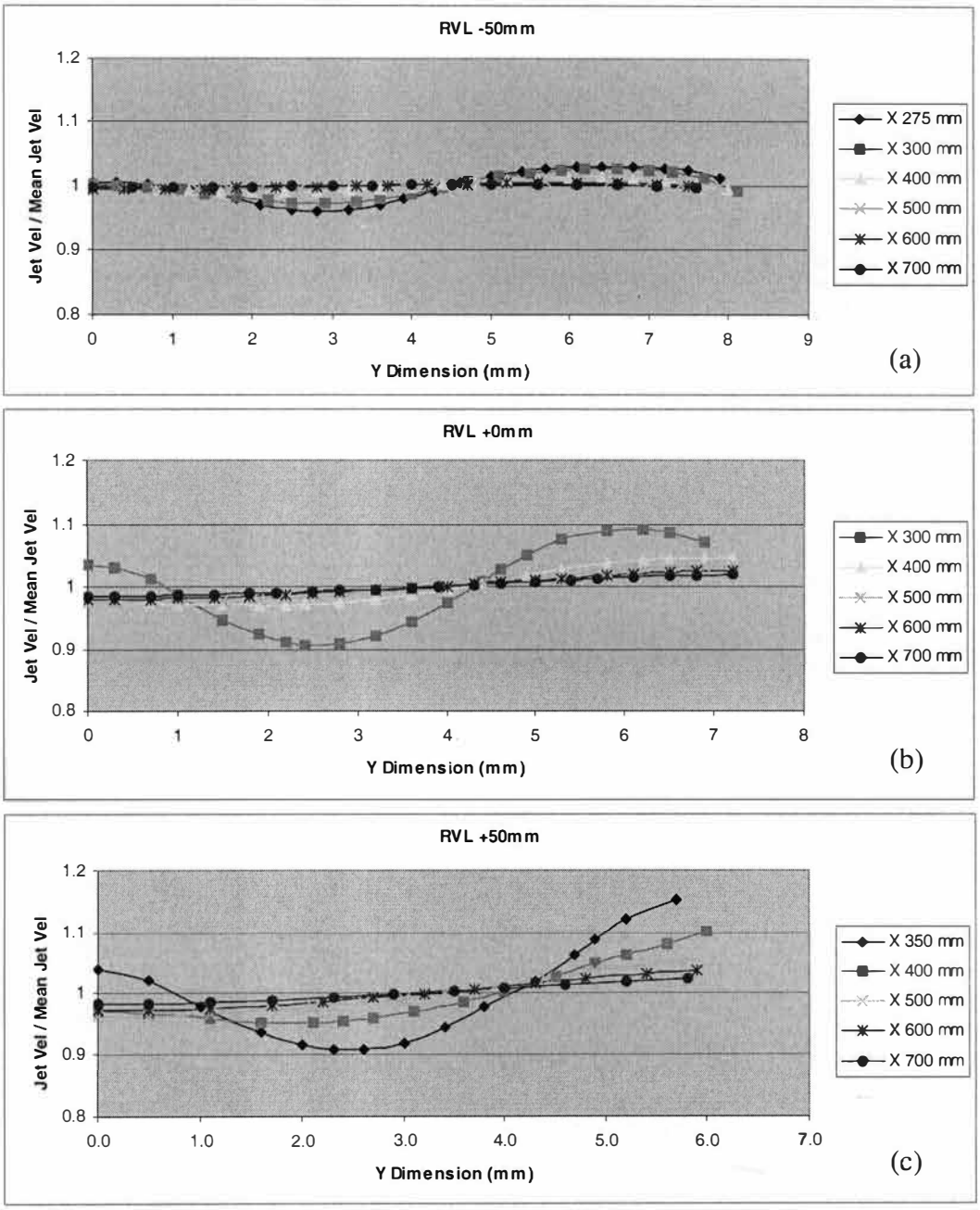

Figure 8. Relative Velocity Profile of Vane Length Case.
(a) RVL = -50 mm.
(b) RVL = +0 mm.
(c) RVL = +50 mm.

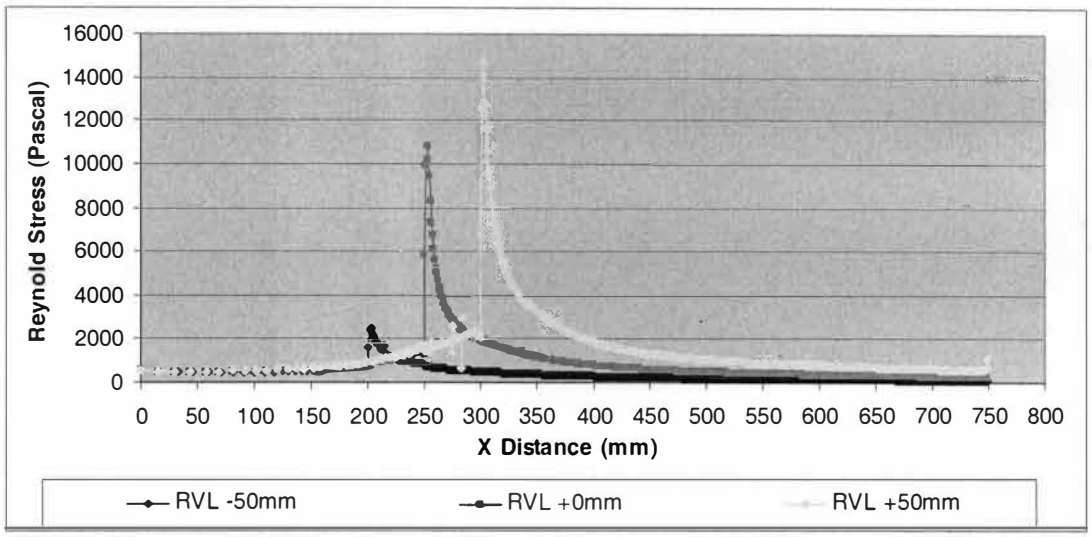

Figure 9. Reynold Stress (Pascal) of Vane Length Case.

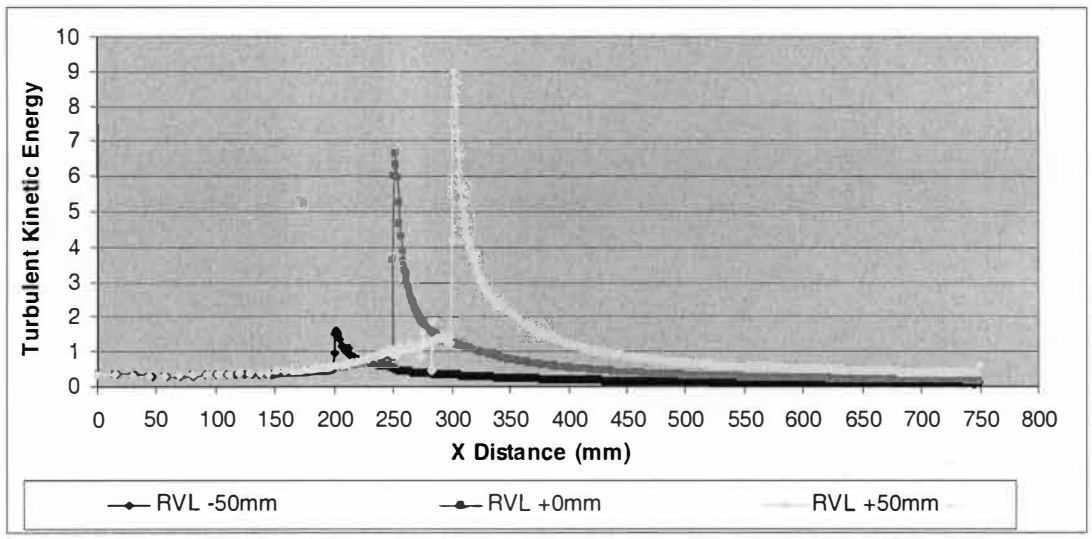

Figure 10. Turbulent Kinetic Energy (m^2/s^2) of Vane Length Case.

The macro scale of turbulence (λ) at the jet plane between the top layer and center layer is plotted versus the horizontal down stream position X for the three cases in Figure 11. Since the horizontal down stream position can be converted to the free jet length, essentially, the figure exhibits that the macro scale of turbulence increases

as the free jet length increases for every case. Smaller scale turbulence generates smaller flocs and less fiber layer mixing around the mixing area between the top and center layers after the vane tip.

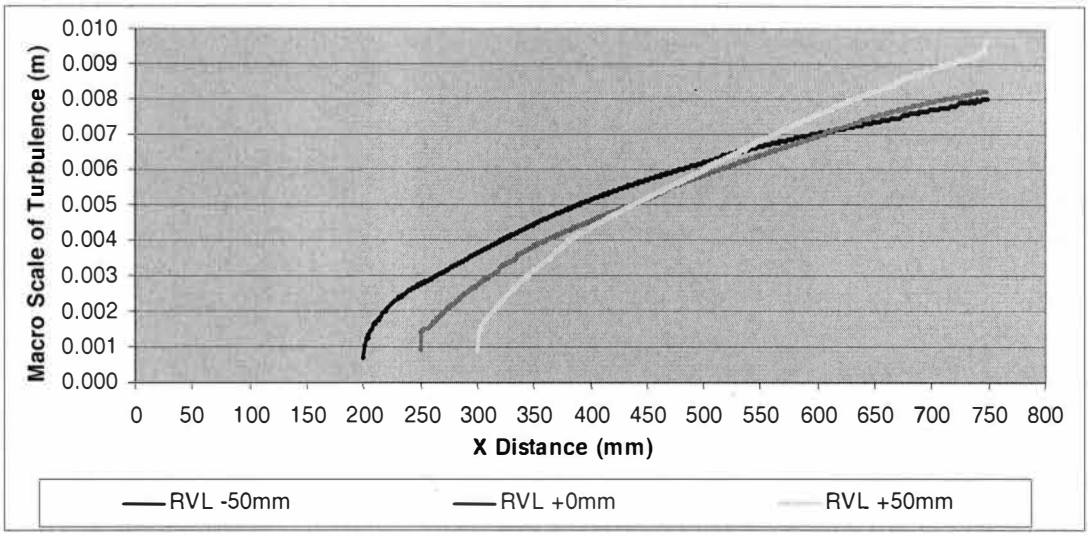

Figure 11. Macro Scale of Turbulence (m) of Vane Length Case.

Physically, the longer free jet could have a longer time for fibers to be mixed and have a higher fiber layer mixing around the mixing area between the top and the center layers in the free jet.

More importantly, when examining the spectrum of macro scale of turbulences for all the three cases with different vane length simultaneously; it appears that the curves in Figure 11 can be roughly divided into two regions along the free jet length. The first region is below X = 500 mm. In this region, the case of RVL= +50 mm has the lowest the macro scale while the case of RVL= -50 mm has the highest macro scale. That is, the case with the longest vane of RVL= +50 mm produces small scale turbulences which lead to less layer mixings. The fibers from the center (inner) layer in this case have a lower possibility to migrate to the top layer of

the sheet. It is surprising that this situation is changed when the free jet length enters the second region that is located above X = 500 mm. The macro scale for the case with RVL= +50 mm continuously grows and becomes the largest one as compared with other two cases. The largest macro scale of turbulence could lead to a strong layer mixing. After systematically examining the results of macro scale of turbulence, Reynolds stress, turbulent kinetic energy, and velocity profile, it is concluded that the case of RVL = +50 mm is the best choice and its free jet length should be less than 250 mm (X < 500 mm). In other words, the jet free length should be controlled within the first region. This results for optimization of vane length are consistent with previous experiments and simulation results [4,10-12]. It appears that the macro scale of turbulence is a very important criterion for optimization of free jet length.

Jet Speed Difference Case

Typically, the turbulent intensity in a headbox is directly proportional to the jet speed. A change in turbulent intensity is assumed to affect the layer mixing. Three cases with different jet speed at 5, 10 and 15 m/s are simulated by using the similar SFH model with RVL= +0 mm as shown in Figure 7(a).

Figure 12, 13 and 14 shows the graphical contour of velocity, turbulent intensity and energy dissipation (ε), respectively, for three cases as mentioned above. They show that the jet velocity, turbulent intensity and energy dissipation increase proportionally with the jet inlet speed.

The results of relative velocity profile along the free jet are plotted in Figure 15. It is clearly shown that the different jet speeds do not affect the decay of wakes. Therefore, the change in jet speed has no effect on the jet outlet profile.

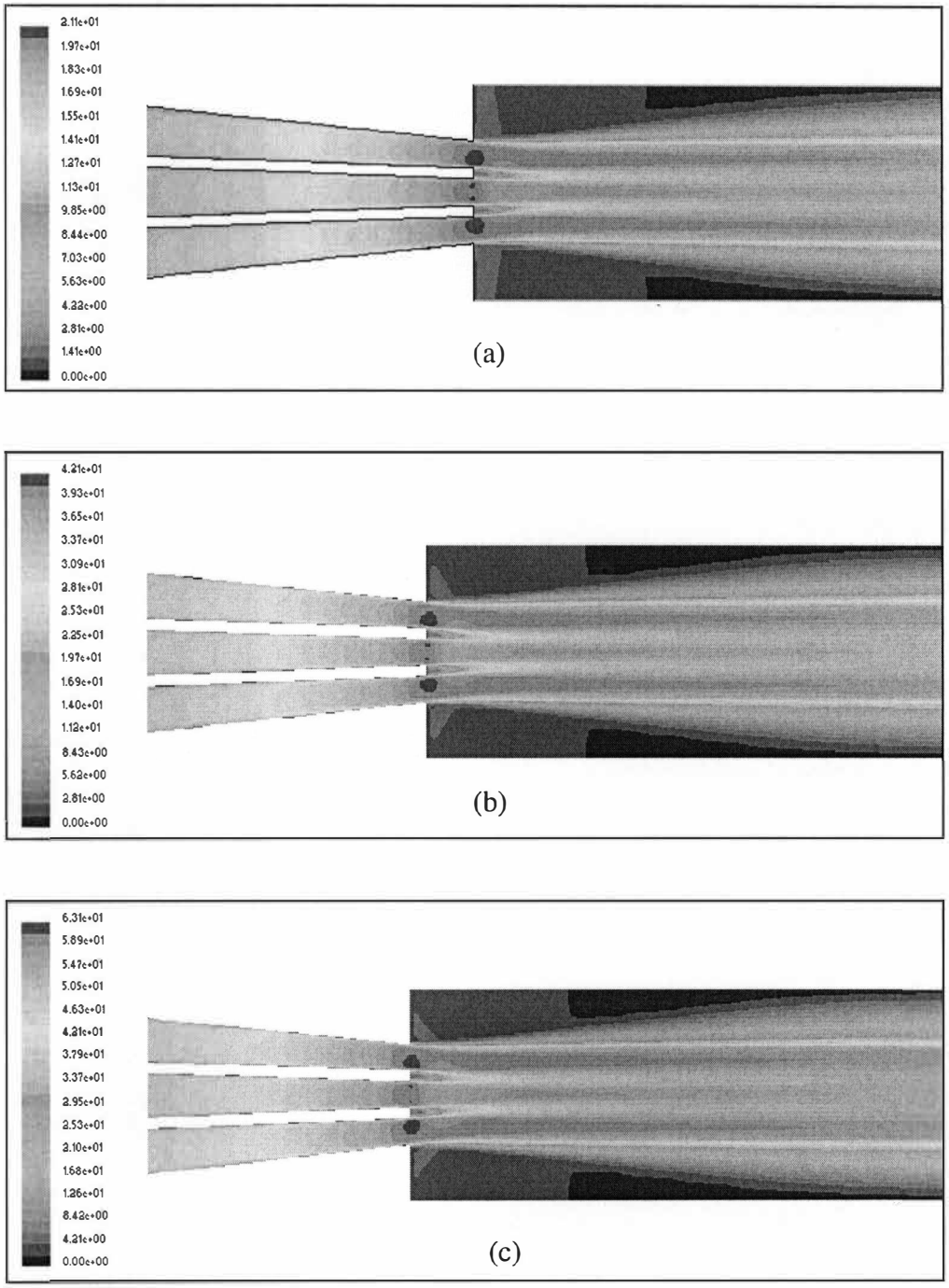

Figure 12. Velocity Contour (m/s) of Different Jet Speed Case.
(a) Jet Inlet Speed 5 m/s.
(b) Jet Inlet Speed 10 m/s.
(c) Jet Inlet Speed 15 m/s.

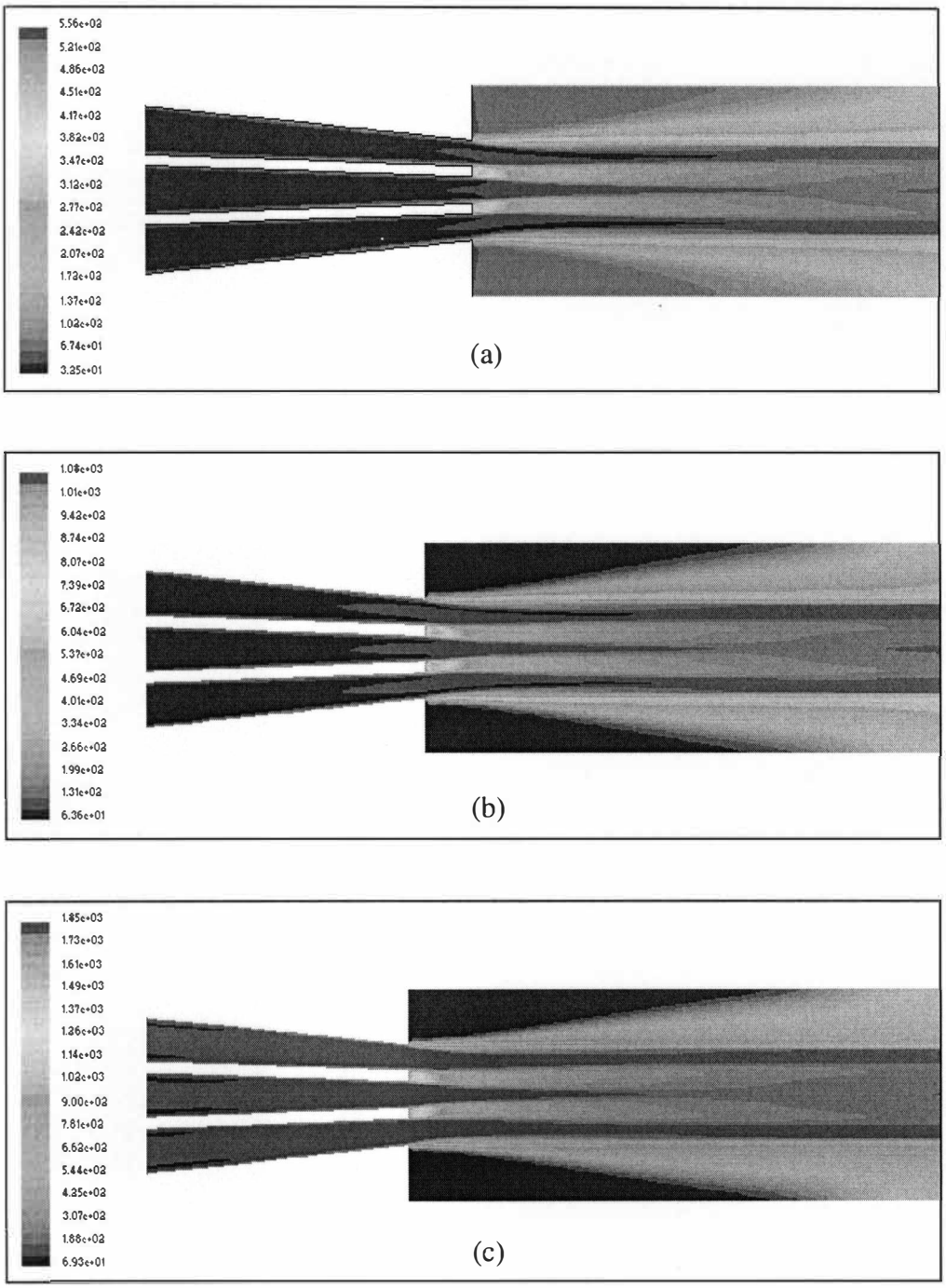

Figure 13. Turbulent Intensity Contour (%) of Different Jet Speed Case.
(a) Jet Inlet Speed 5 m/s.
(b) Jet Inlet Speed 10 m/s.
(c) Jet Inlet Speed 15 m/s.

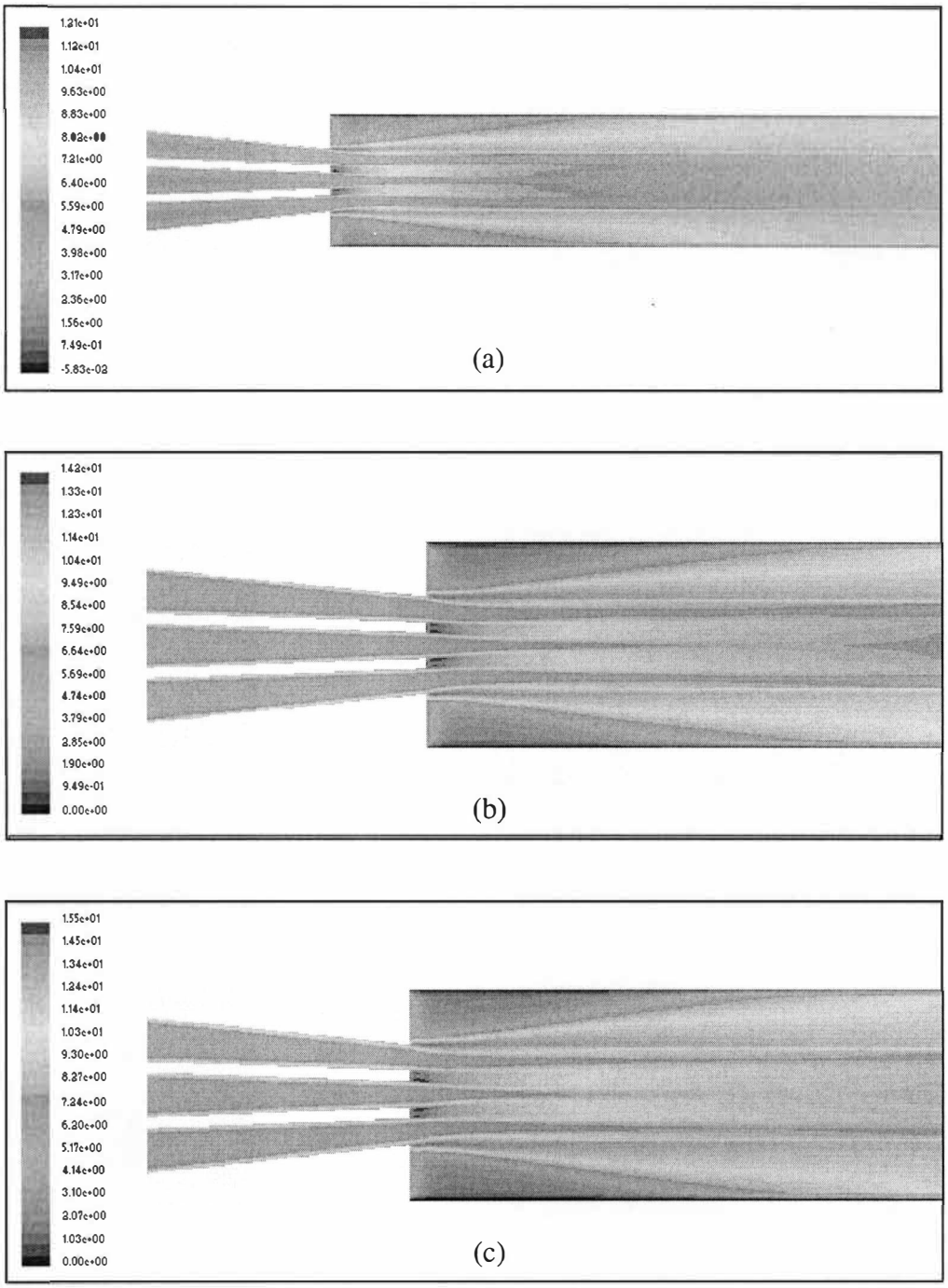

Figure 14. Energy Dissipation (m^2/s^3) Contour of Different Jet Speed Case in Logarithmic Scale.
(a) Jet Inlet Speed 5 m/s.
(b) Jet Inlet Speed 10 m/s.
(c) Jet Inlet Speed 15 m/s.

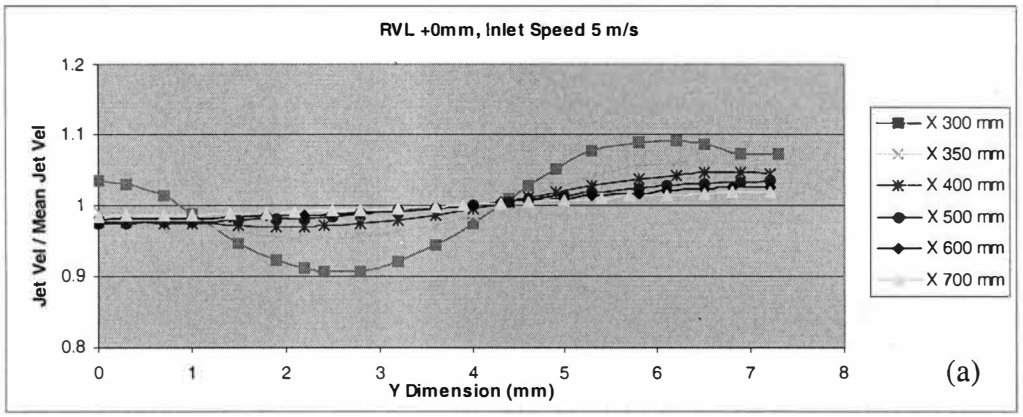

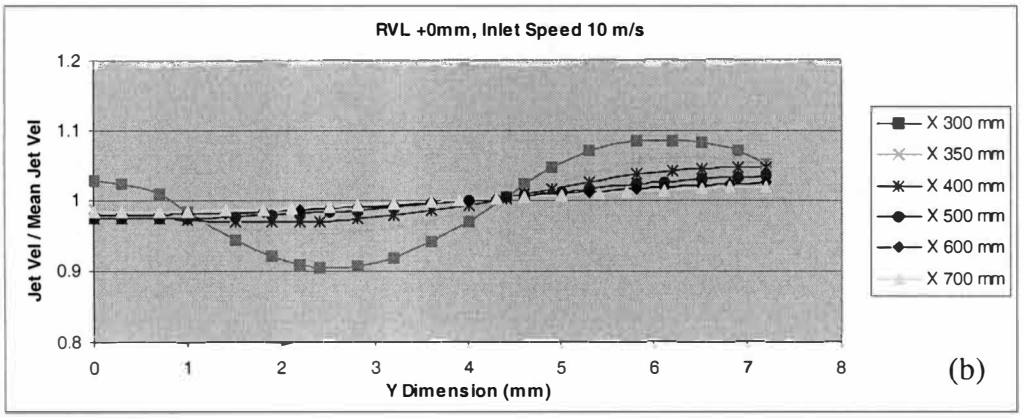

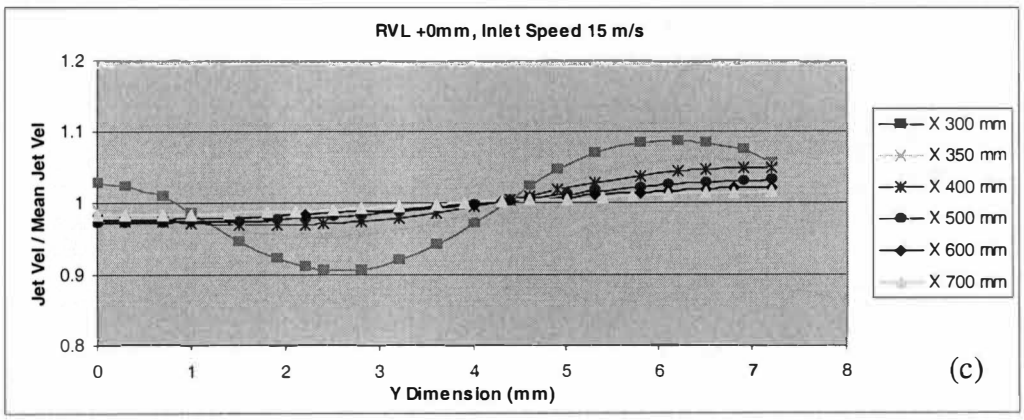

Figure 15. Relative Velocity Profile of Different Jet Speed Case.
(a) Jet Speed Inlet 5 m/s.
(b) Jet Speed Inlet 10 m/s.
(c) Jet Speed Inlet 15 m/s.

The average Reynolds stress and turbulent kinetic energy as a function of horizontal down stream position X are shown in Figure 16 and 17, respectively. The higher jet speed inlet produces the higher Reynolds stress and turbulent kinetic energy inside the headbox and in the free jet. These different levels of turbulence are expected to give different levels of layer mixing.

However, the different jet inlet speeds give approximately the similar macro scale of turbulence as shown in Figure 18. That means the change in turbulent level from different jet speed has no any effect on the macro scale of turbulence or the layer mixing. This simulation outcome is consistent with the previous experiments [10-11,13]. Therefore, the variation of jet speed during operation does not affect the layer mixing of SFH.

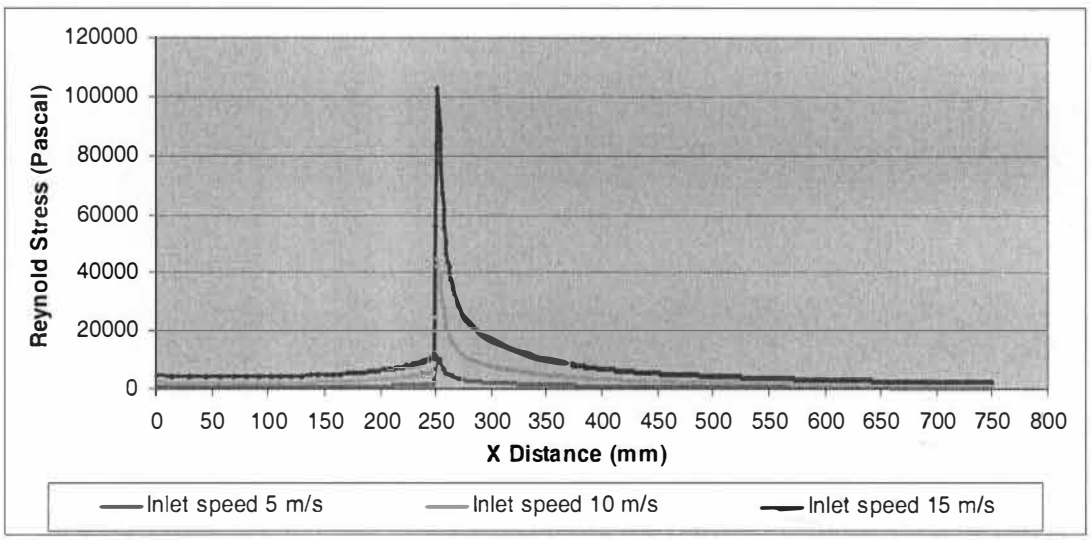

Figure 16. Reynolds Stress (Pascal) of Different Jet Speed Case.

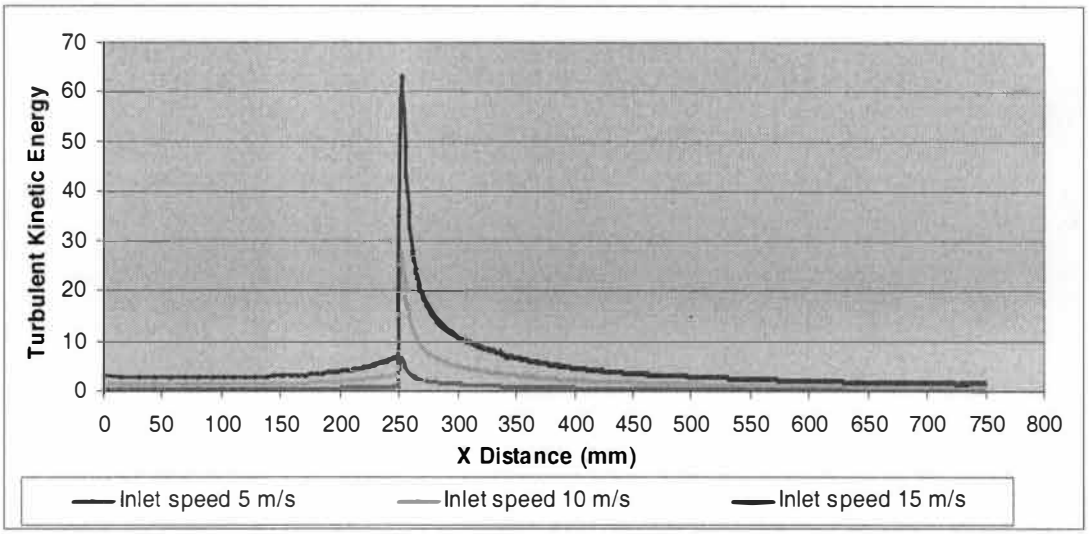

Figure 17. Turbulent Kinetic Energy (m^2/s^2) of Different Jet Speed Case.

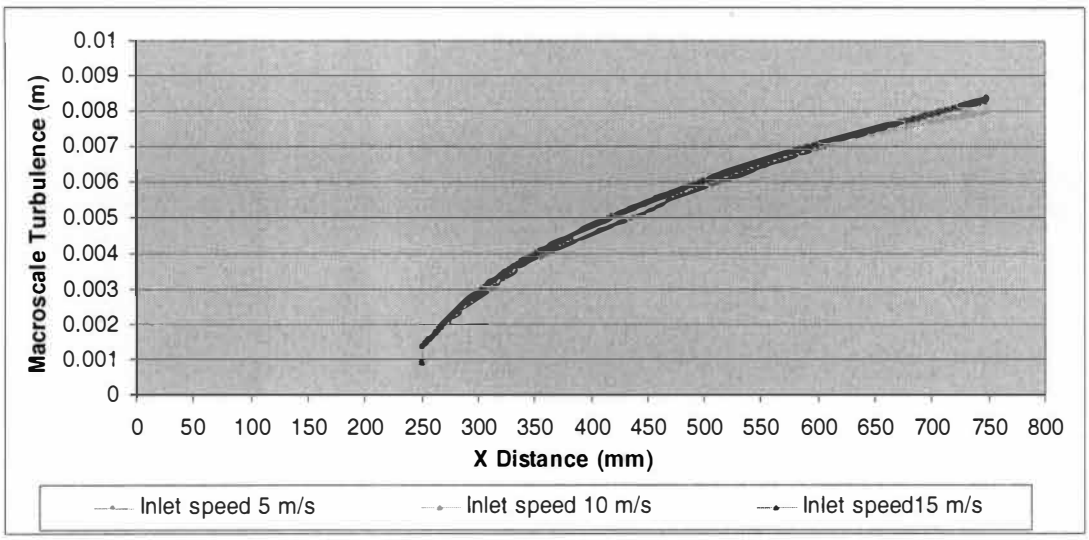

Figure 18. Macro Scale of Turbulence (m) of Different Jet Speed Case.

Vane Thickness Case

The three SFH models with vane thickness 1, 2 and 3 mm are simulated for optimization in this case. The slice opening of these three models is fixed at 5

mm/layer to eliminate the effect of the slice opening. The headbox models of vane thickness 1 and 3 mm are shown in Figure 19(a) and 19(b), respectively.

The graphical contours of turbulent intensity and energy dissipation are shown in Figure 20 and 21. These figures show that the magnitude of turbulent intensity and energy dissipation are approximately equal in all three models. However, the turbulence produced by the thicker vane has larger scale than the thinner vane as it covers a larger area of the layer mixing after the vane tip. Therefore, it can be concluded that the magnitude of turbulence intensity depends on the jet speed, while the size of turbulence depends on the wake area or the thickness of the vane.

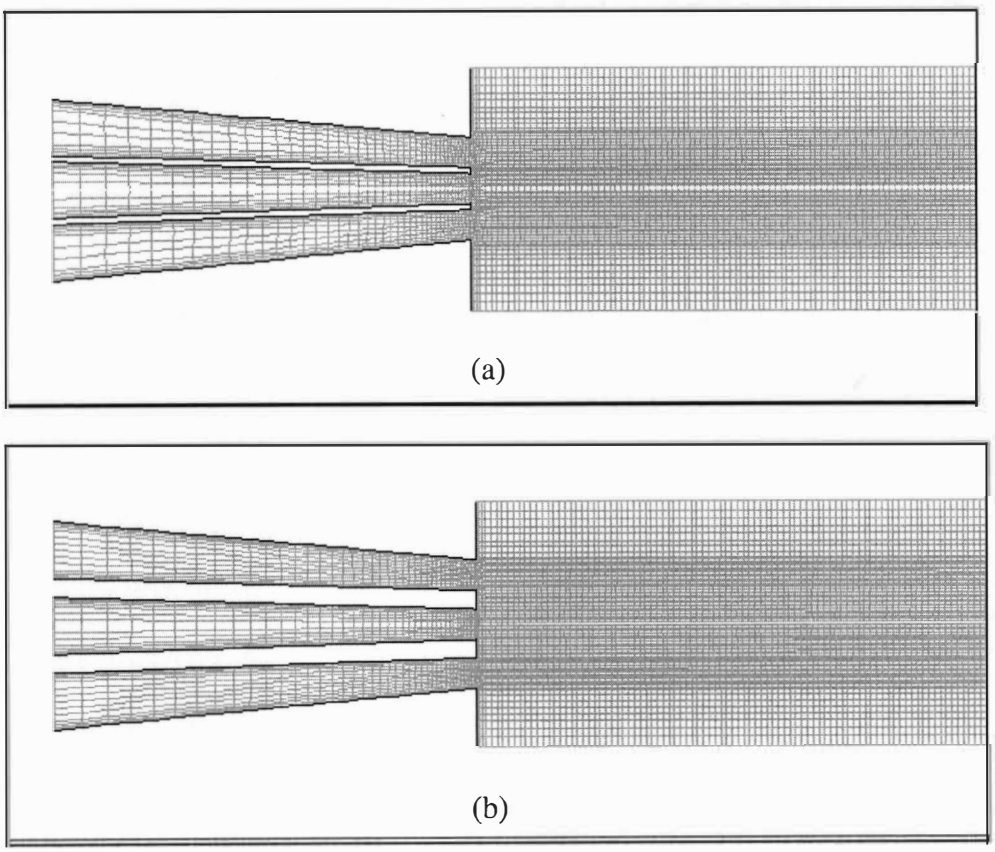

Figure 19. Headbox Models of Vane Thickness Case.
(a) Vane Thickness 1 mm.
(b) Vane Thickness 3 mm.

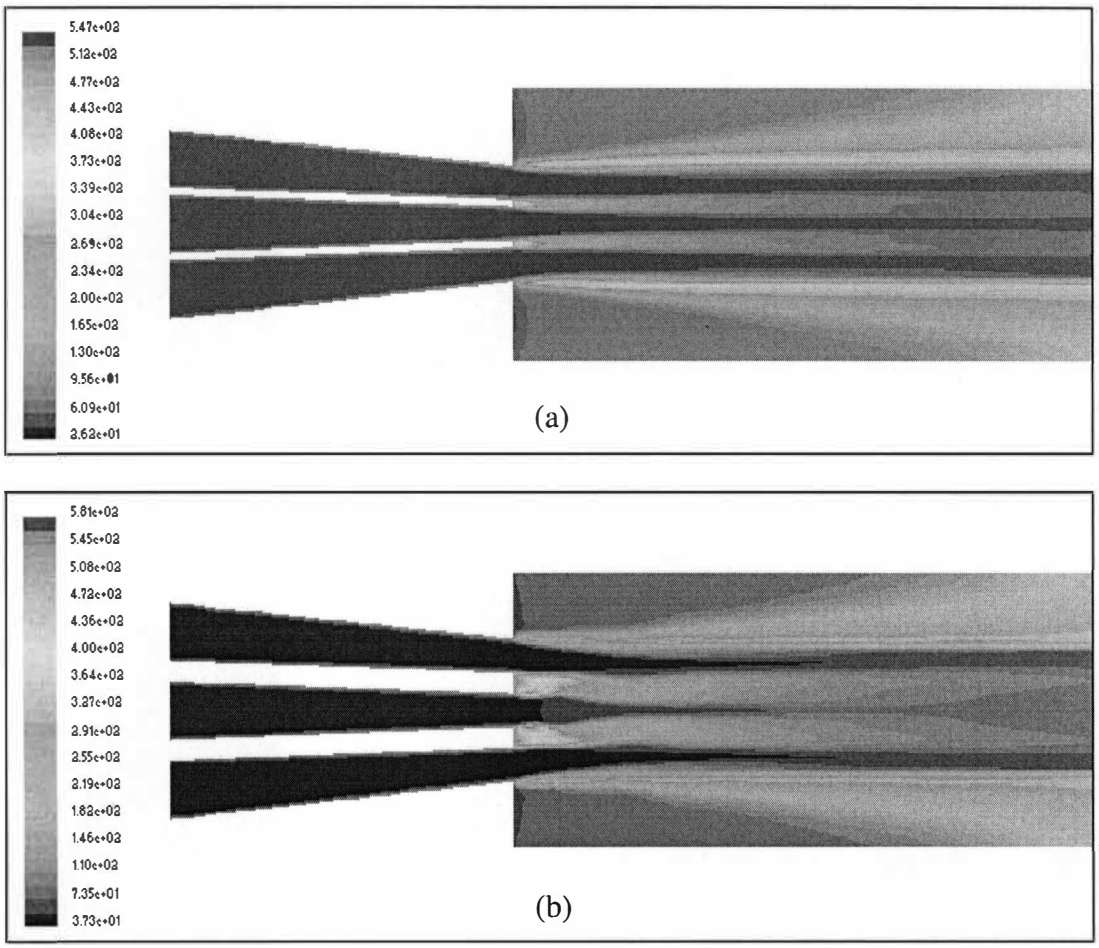

Figure 20. Contour of Turbulent Intensity (%) of Vane Thickness Case.
(a) Vane Thickness 1 mm.
(b) Vane Thickness 3 mm.

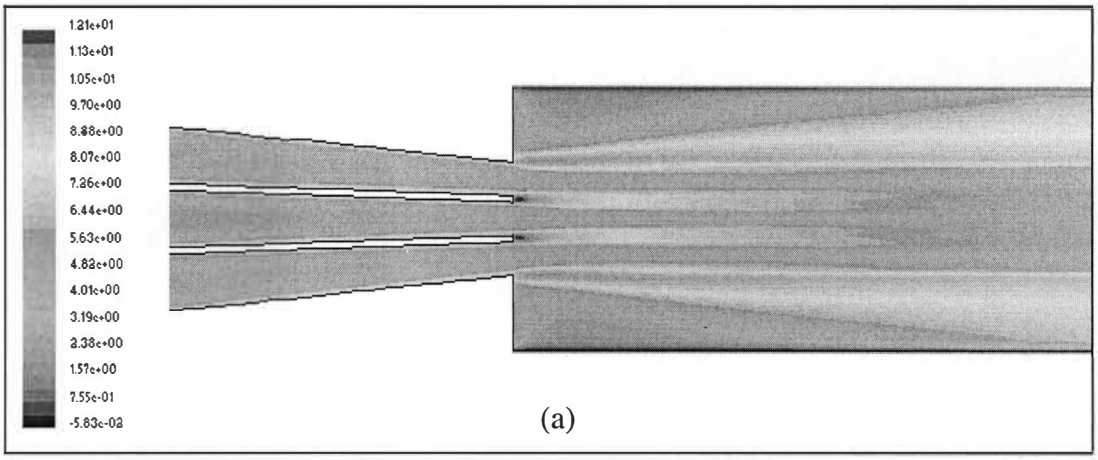

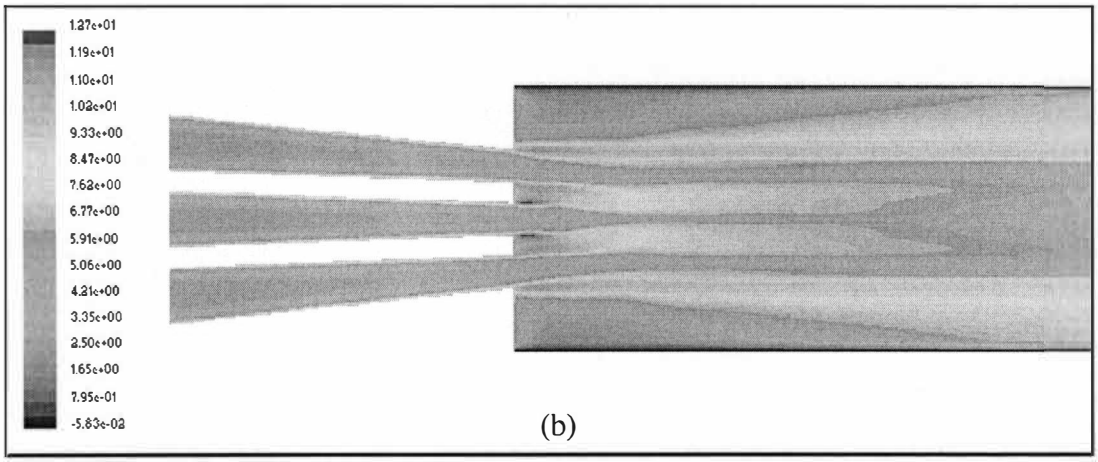

Figure 21. Energy Dissipation (m^2/s^3) Contour of Different Jet Speed Case in Logarithmic Scale.
(a) Vane Thickness 1 mm.
(b) Vane Thickness 3 mm.

According to the relative velocity profile plot in Figure 22, the thinner vane produces the most uniform velocity profile in this case. From Figure 23 and 24, Reynolds stress and turbulent kinetic energy of different vane thicknesses are equal inside the headbox. Due to the larger wake area, the thicker vane produces more intense turbulence after the vane tip. This more intense turbulence gives the non-uniform velocity profile and tends to increase the layer mixing in the free jet.

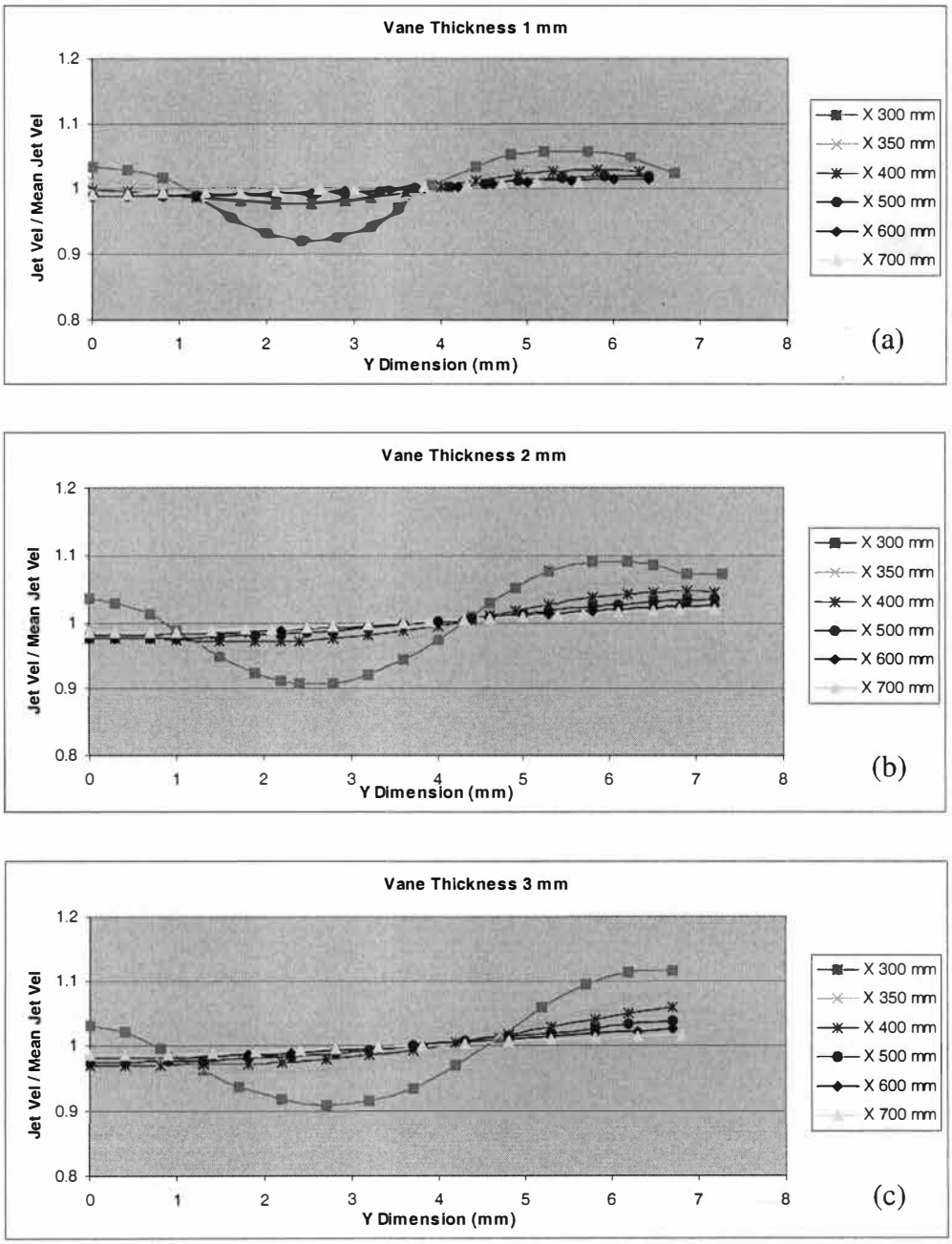

Figure 22. Relative Velocity Profile of Vane Thickness Case.
(a) Vane Thickness 1 mm.
(b) Vane Thickness 2 mm.
(c) Vane Thickness 3 mm.

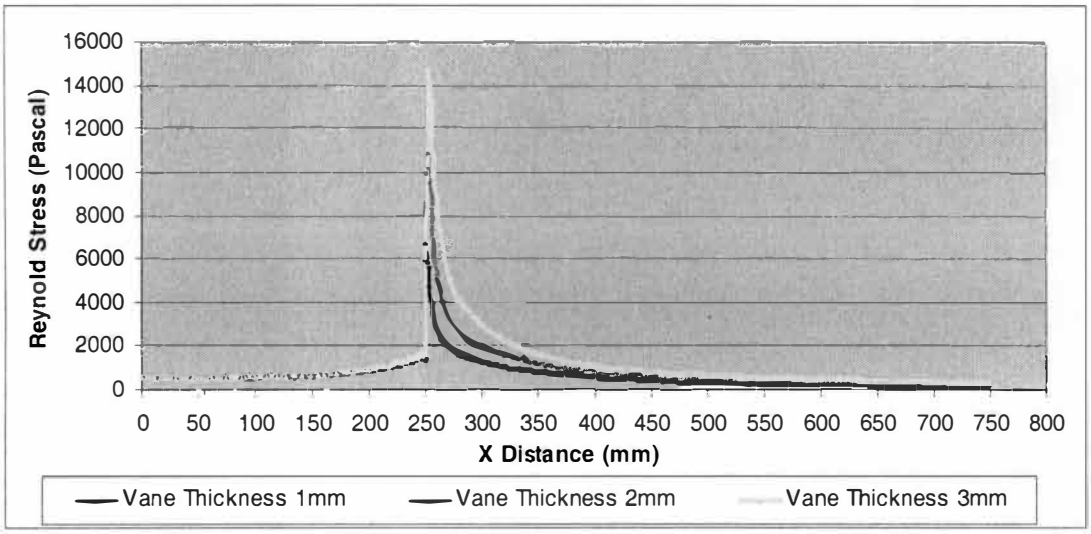

Figure 23. Reynolds Stress (Pascal) of Vane Thickness Case.

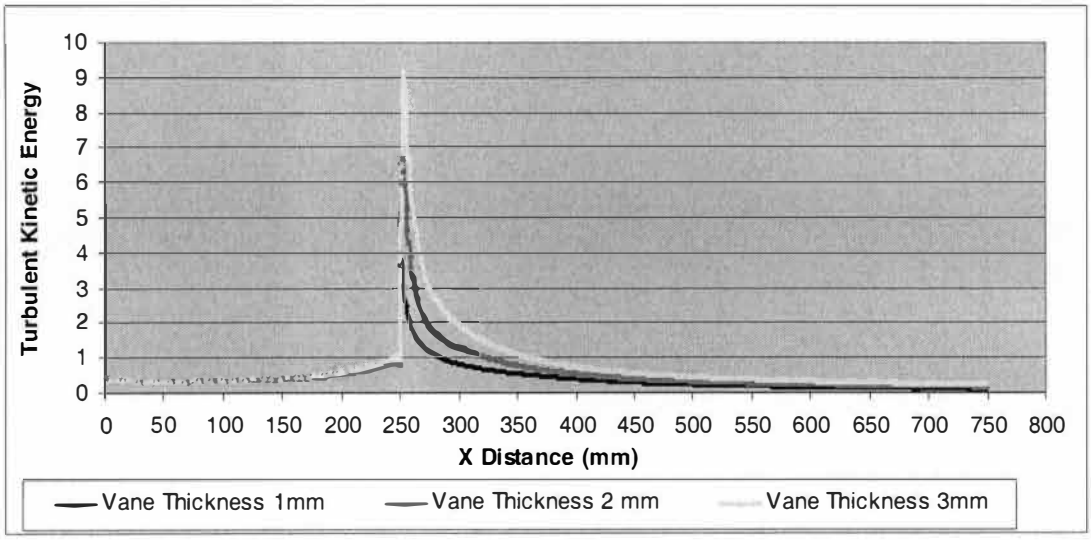

Figure 24. Turbulent Kinetic Energy (m^2/s^2) of Vane Thickness Case.

The macro scale of turbulence at the jet plane between the top and center layer is plotted for three cases in Figure 25. It is clearly shown that the thicker the vane is, the larger the macro scale of turbulence is, due to the layer mixing in the wake area behind the vane. Not only does the thicker vane produce the more intense turbulence

and non-uniform velocity profile in the free jet, but it also generates the large scale of turbulence that results in more layers mixing.

From this result, the case with the thin vane (1 mm) gives the lowest layer mixing and more uniform jet velocity profile. Therefore, the thin vane is preferred in stratified headbox to produce the fine scale of turbulence giving a better surface property.

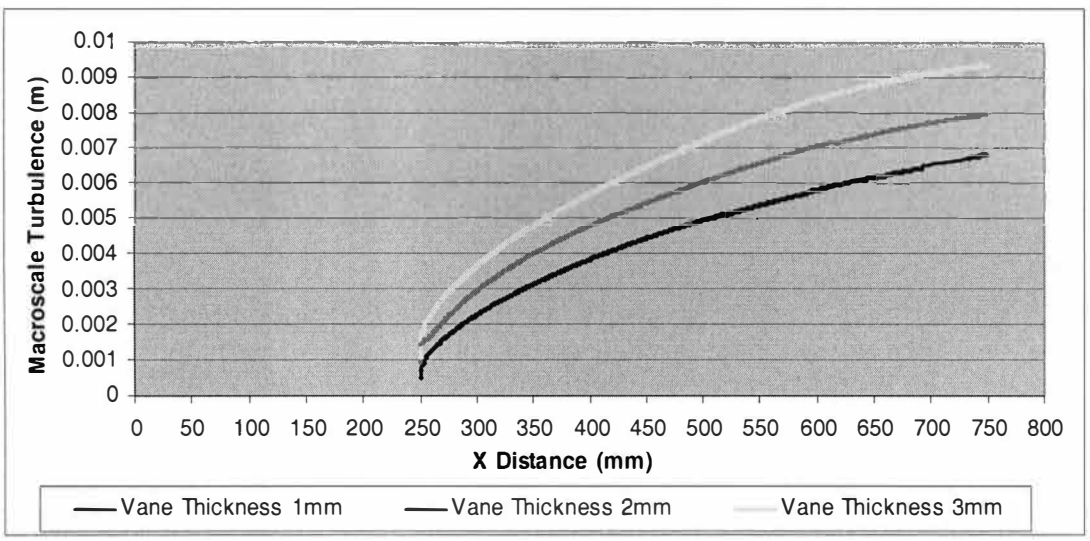

Figure 25. Macro Scale of Turbulence (m) of Vane Thickness Case.

Headbox Angle Case

In this case, the inlet width of each layer in this case is varied to obtain different headbox angles. While keeping the slice opening constant, the effect of slice opening is excluded from this simulation. The velocity in the inlet is adjusted to have the same average jet velocity in the outlet. The headbox models with angle variation are shown in Figure 26.

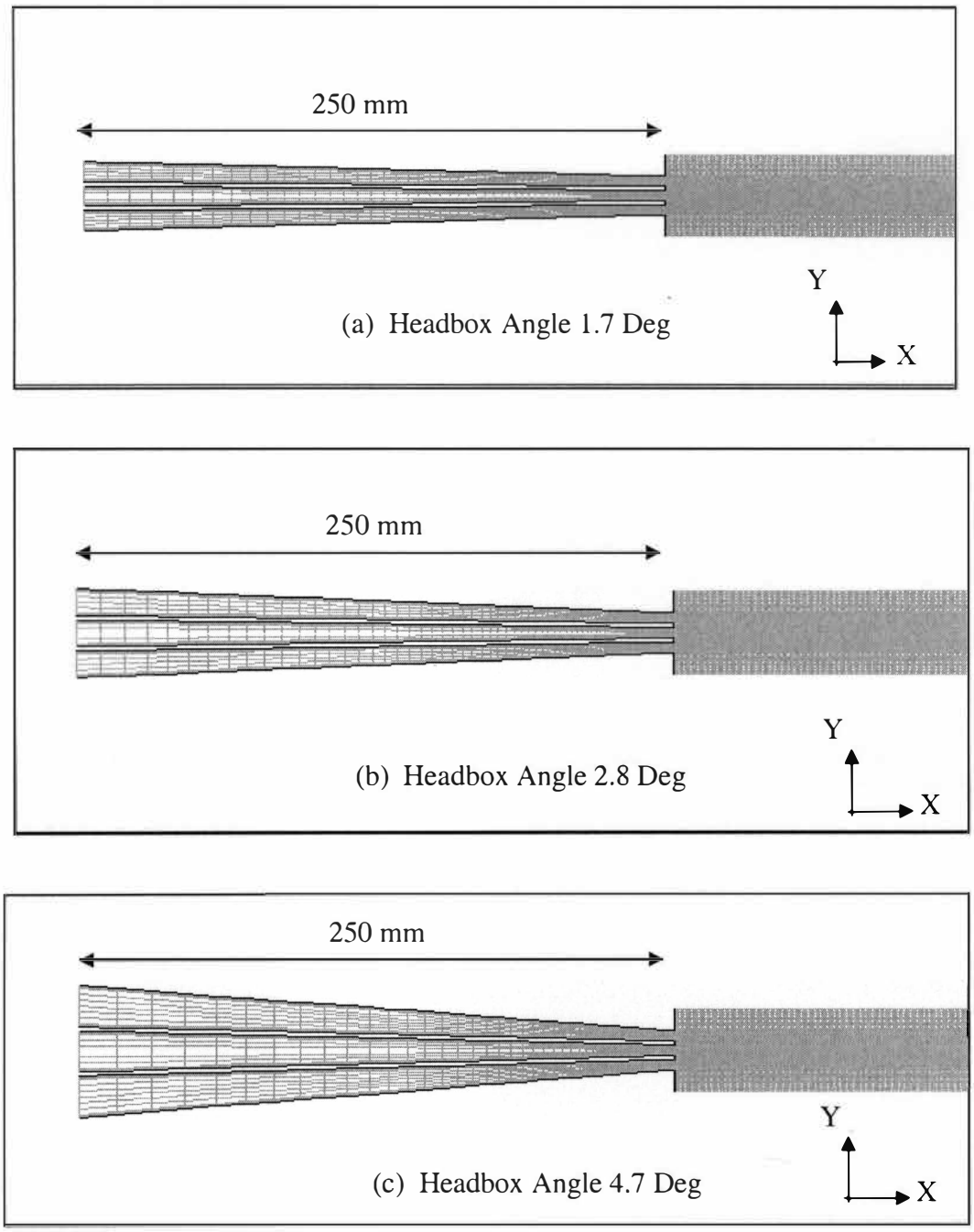

Figure 26. Headbox Models of Headbox Angle Case.
(a) Headbox Angle 1.7 Deg.
(b) Headbox Angle 2.8 Deg.
(c) Headbox Angle 10.2 Deg.

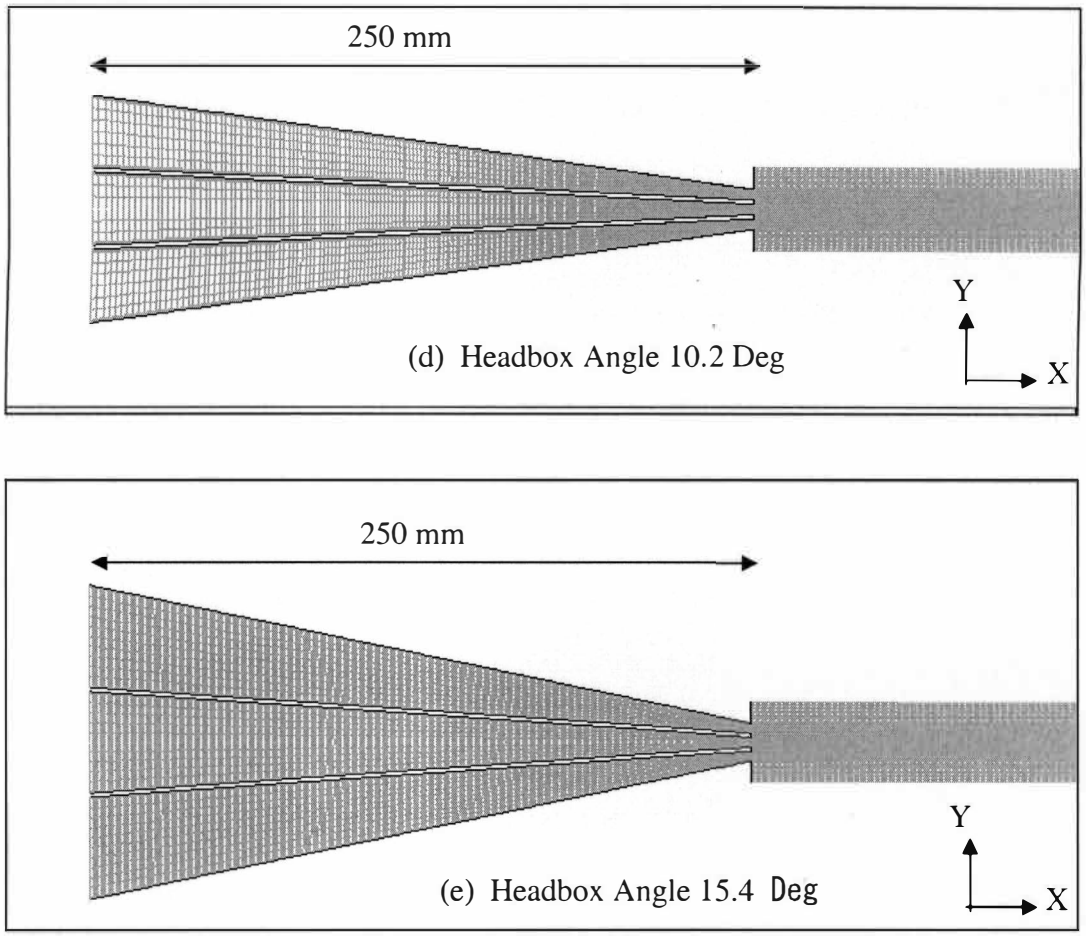

Figure 26. Headbox Models of Headbox Angle Case. (Continued)
(d) Headbox Angle 10.2 Deg.
(e) Headbox Angle 15.4 Deg.

From the plots of relative velocity profile in Figure 27, it is found that the increase in headbox angle gives the better uniform of velocity profile. The lower velocity in the inlet with the higher headbox angle reduces the effect of the wake area behind the vane, as the result of the more uniform velocity profile.

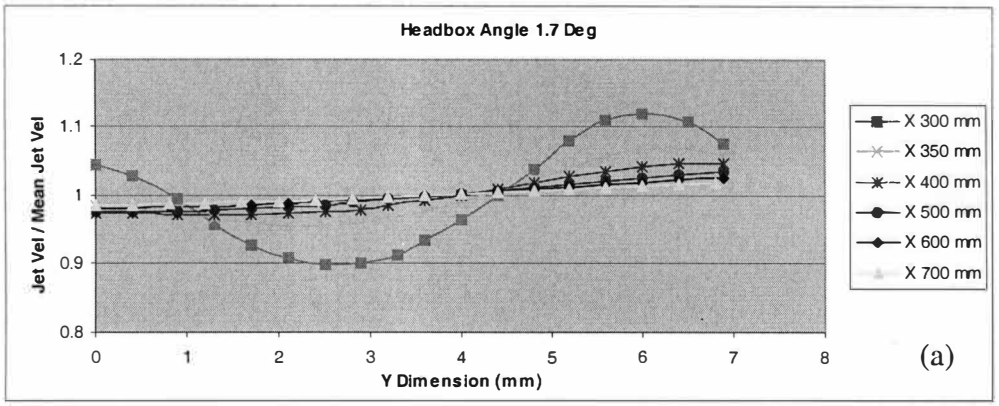

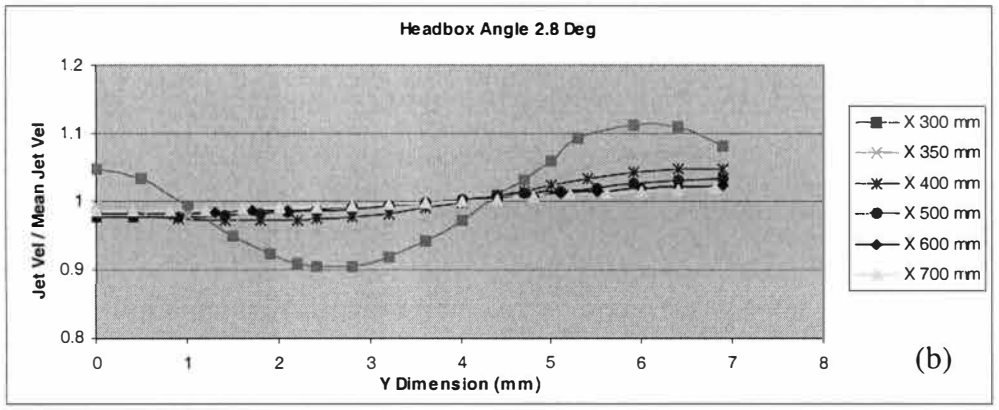

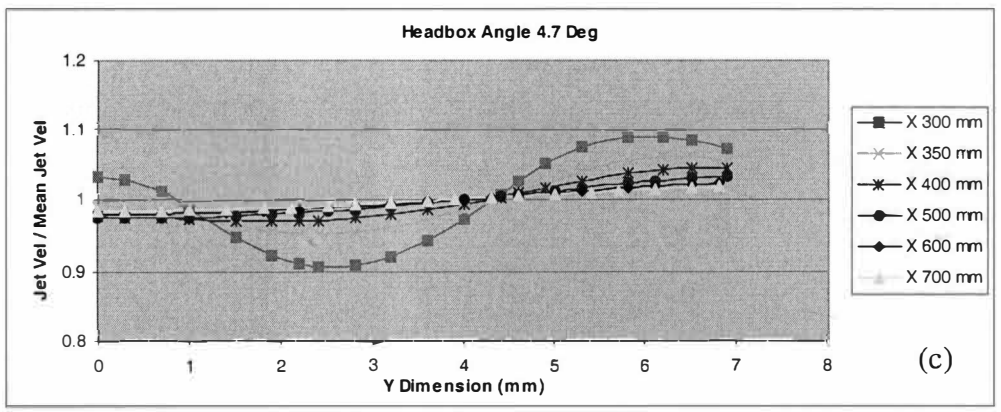

Figure 27. Relative Velocity Profile of Headbox Angle Case.
(a) Headbox Angle 1.7 Deg.
(b) Headbox Angle 2.8 Deg.
(c) Headbox Angle 4.7 Deg.

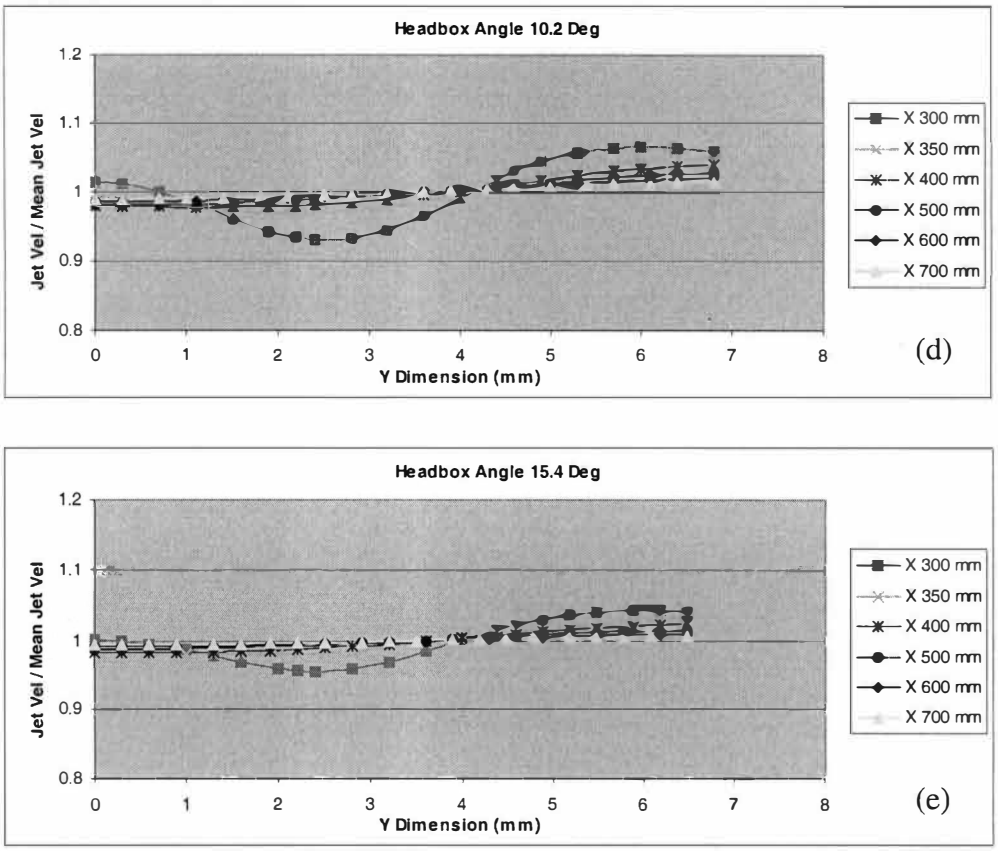

Figure 27. Relative Velocity Profile of Headbox Angle Case. (Continued)
(d) Headbox Angle 10.2 Deg.
(e) Headbox Angle 15.4 Deg.

Reynolds stress and turbulent kinetic energy inside the headbox (X < 250 mm) increase as the headbox angle decreases, while the Reynolds stress and turbulent kinetic energy in the free jet (X > 250mm) are not significantly affected by the variation of angles as shown in Figure 28 and 29, respectively. The lower headbox angle produces the higher turbulent shear force inside the headbox (X < 250 mm) to break down the flocs in each fiber layer.

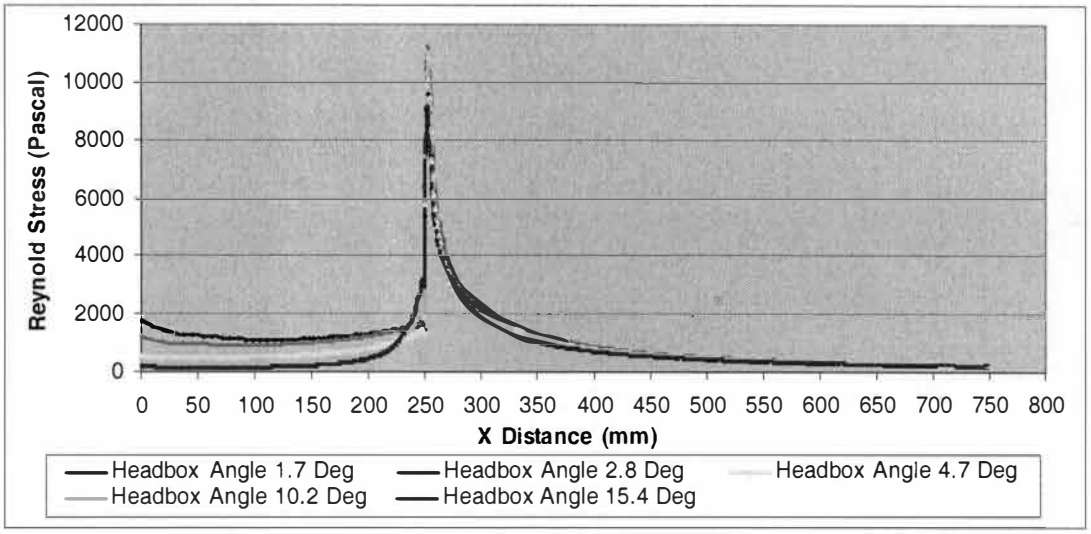

Figure 28. Reynolds Stress (Pascal) of Headbox Angle Case.

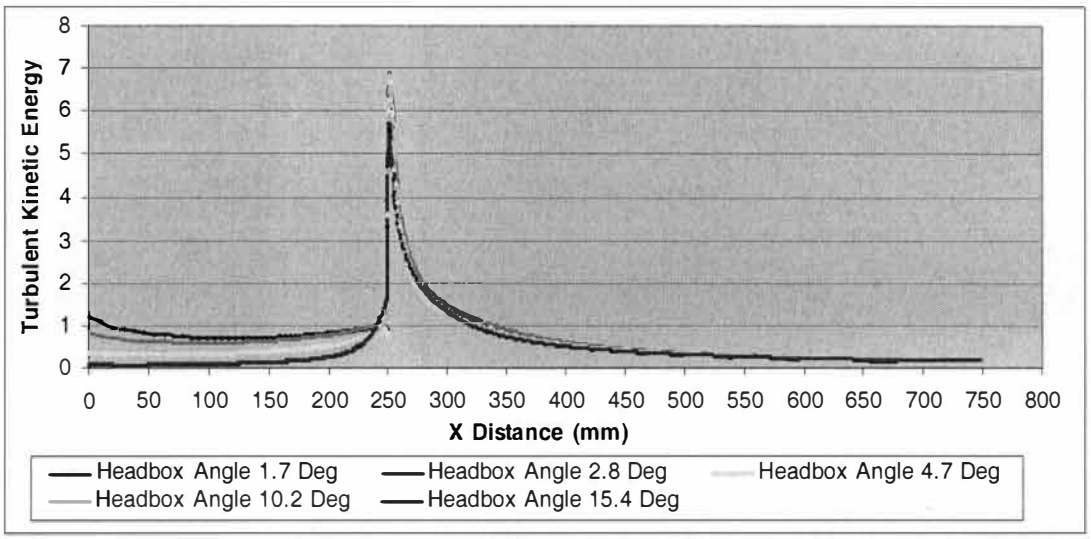

Figure 29. Turbulent Kinetic Energy (m^2/s^2) of Headbox Angle Case.

In contrary, Figure 30 shows that the headbox with angle 4.7 degrees has the lowest macro scale of turbulence, i.e. the lowest layer mixing. In case of the headboxes with angles 1.7 and 2.8 degrees, the higher turbulence level inside the headbox may possibly cause higher layer mixing. Therefore, it can be concluded that

the angle of headbox should be optimized in order to produce the lowest layer mixing level. From this simulation, the optimum headbox angle is 4.7 degrees. However, this simulation result for headbox angle is different from that by Parsheh and Dahlkild [4]. Their optimum headbox angle is 8 through 12 degrees. This difference may come from the different design of stratified headbox used in simulation.

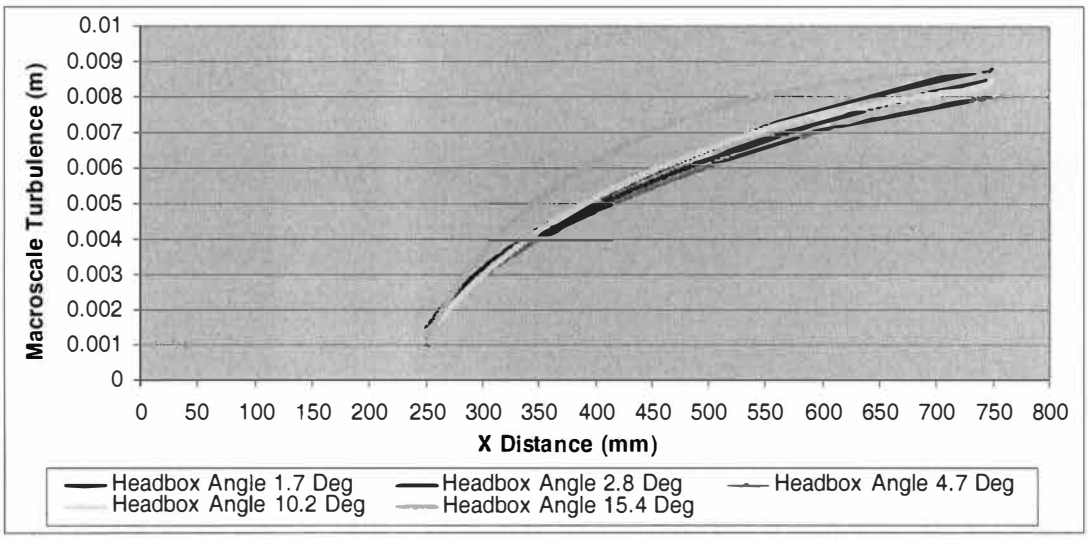

Figure 30. Macro Scale of Turbulence (m) of Headbox Angle Case.

Slice Opening Case

Typically, when the slice opening varies, the angle of the vane and headbox is changed. This effect is a normal operating condition of paper machine operation; therefore, the vane and headbox angles are changed as the slice opening varies. The velocity in the inlet is adjusted to have the same average jet velocity in the outlet. In this case, four headboxes with 4, 5, 7.5 and 10 mm opening per layer are simulated to investigate the effect of slice opening on layer mixing. The graphics of headbox models are shown in Figure 31.

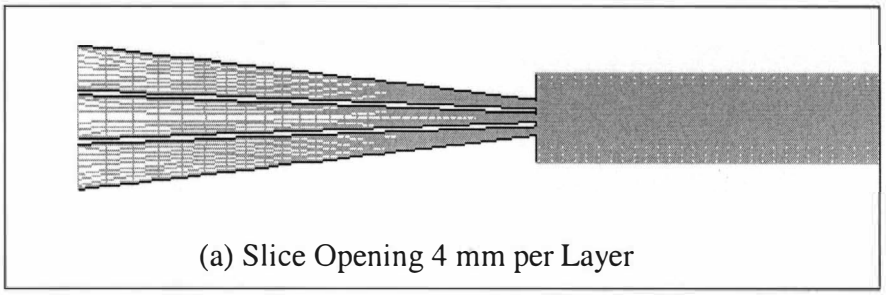

(a) Slice Opening 4 mm per Layer

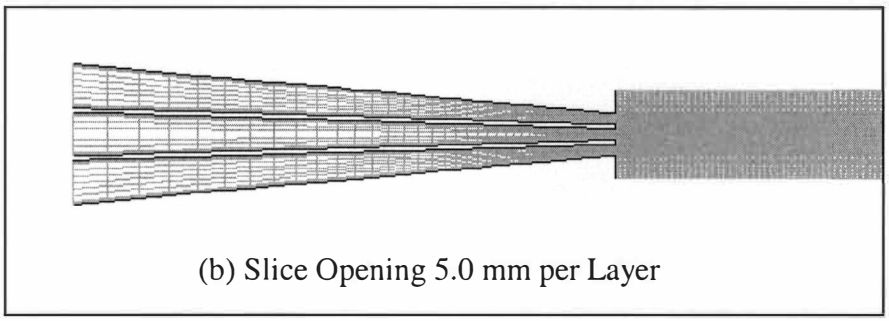

(b) Slice Opening 5.0 mm per Layer

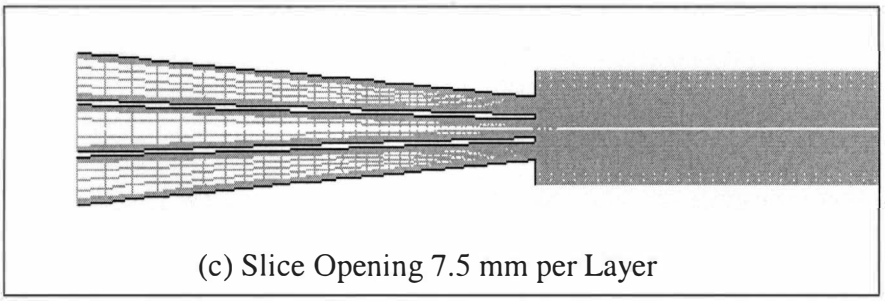

(c) Slice Opening 7.5 mm per Layer

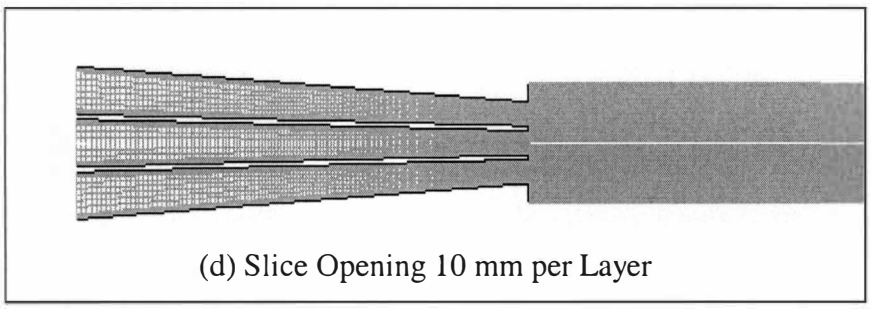

(d) Slice Opening 10 mm per Layer

Figure 31. Headbox Models of Slice Opening Case.
(a) Total Slice Opening 16.0 mm. (4 mm per layer).
(b) Total Slice Opening 19.0 mm. (5 mm per layer).
(c) Total Slice Opening 26.5 mm. (7.5 mm per layer).
(d) Total Slice Opening 34.0 mm. (10 mm per layer).

The contours of turbulent intensity and energy dissipation are shown in Figure 32 and 33, respectively. Average Reynolds stress and turbulent kinetic energy are shown in Figure 35 and 36, respectively. They show that the wider slice opening has the higher turbulent level inside the headbox (X < 250 mm). This effect is caused by the higher velocity in the inlet of the wider slice opening. However, the low intense turbulence in narrower slice opening gives more uniform velocity profile as shown in Figure 34.

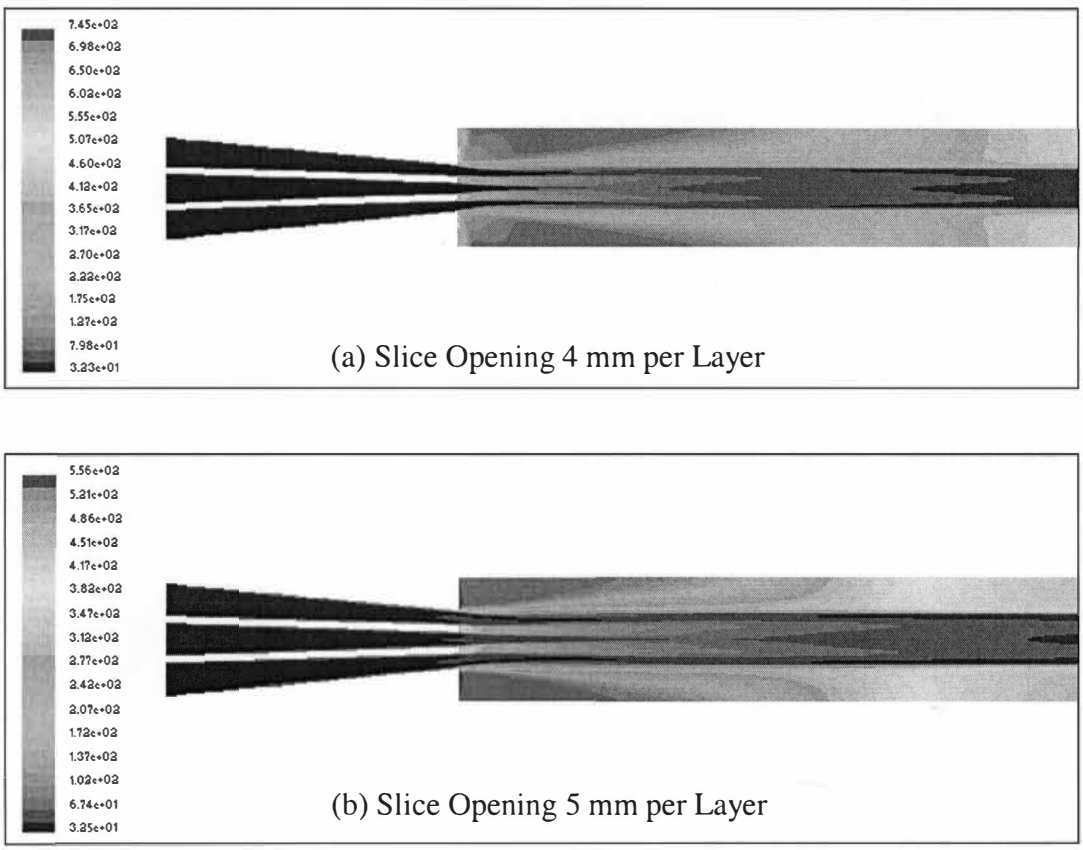

Figure 32. Contour of Turbulent Intensity (%) of Slice Opening Case.
(a) Total Slice Opening 16.0 mm. (4 mm per layer).
(b) Total Slice Opening 19.0 mm. (5 mm per layer).

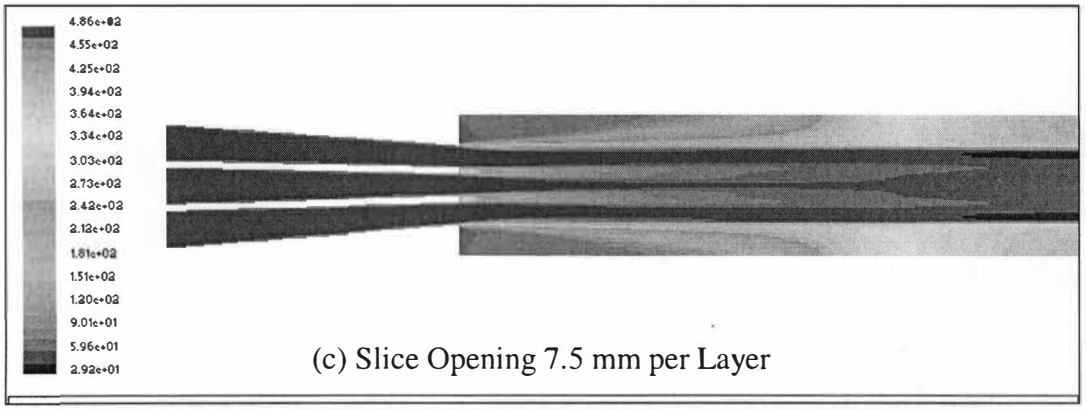

(c) Slice Opening 7.5 mm per Layer

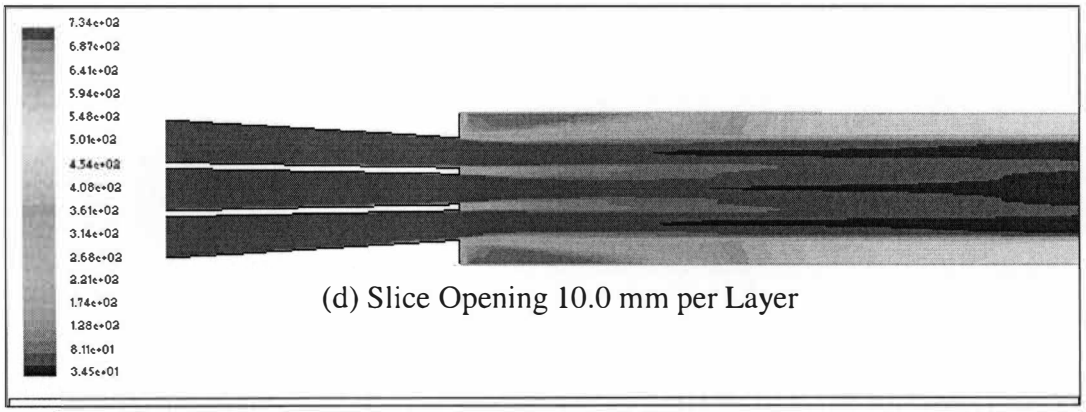

(d) Slice Opening 10.0 mm per Layer

Figure 32. Contour of Turbulent Intensity (%) of Slice Opening Case. (Continued)
(c) Total Slice Opening 26.5 mm. (7.5 mm per layer).
(d) Total Slice Opening 34.0 mm. (10 mm per layer).

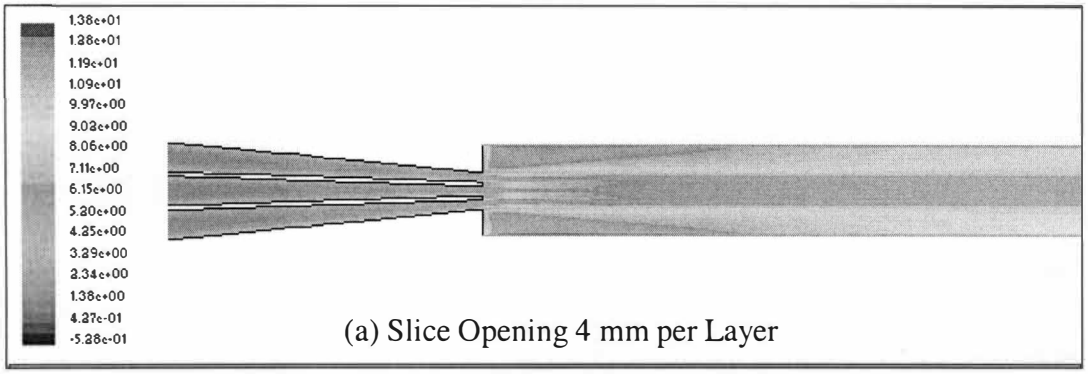

(a) Slice Opening 4 mm per Layer

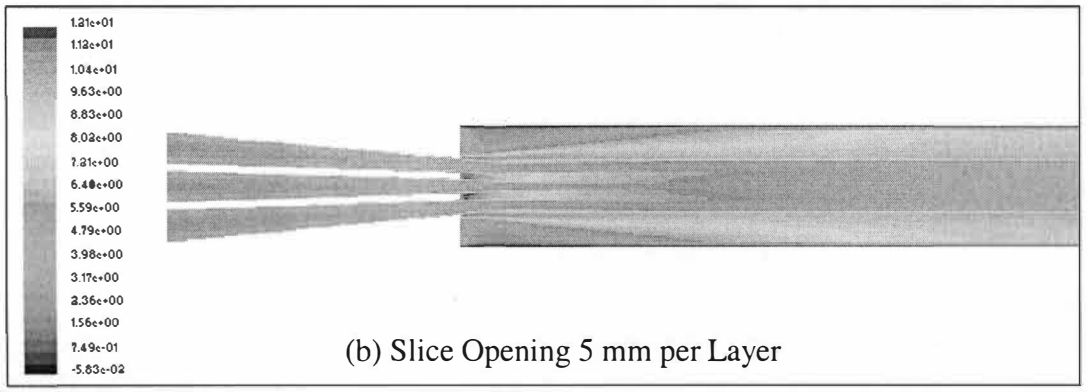

(b) Slice Opening 5 mm per Layer

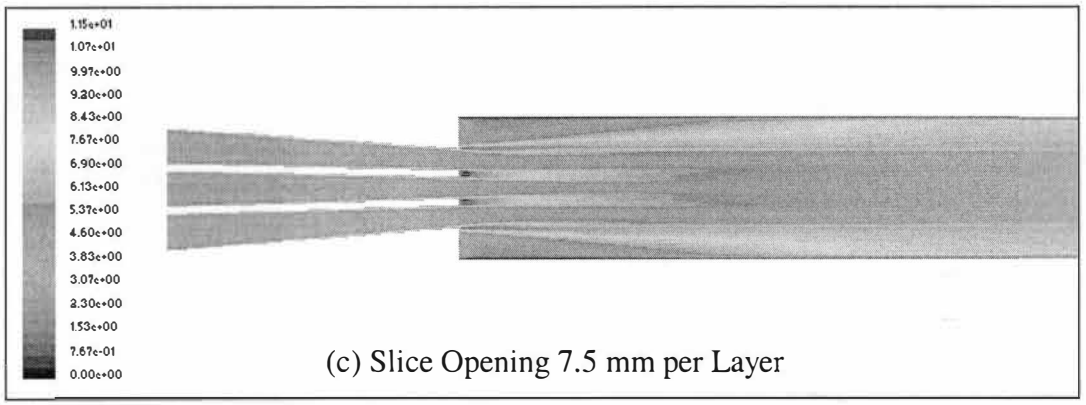

(c) Slice Opening 7.5 mm per Layer

Figure 33. Energy Dissipation (m^2/s^3) Contour of Slice Opening Case in Logarithmic Scale.
(a) Total Slice Opening 16.0 mm. (4 mm per layer).
(b) Total Slice Opening 19.0 mm. (5 mm per layer).
(c) Total Slice Opening 26.5 mm. (7.5 mm per layer).

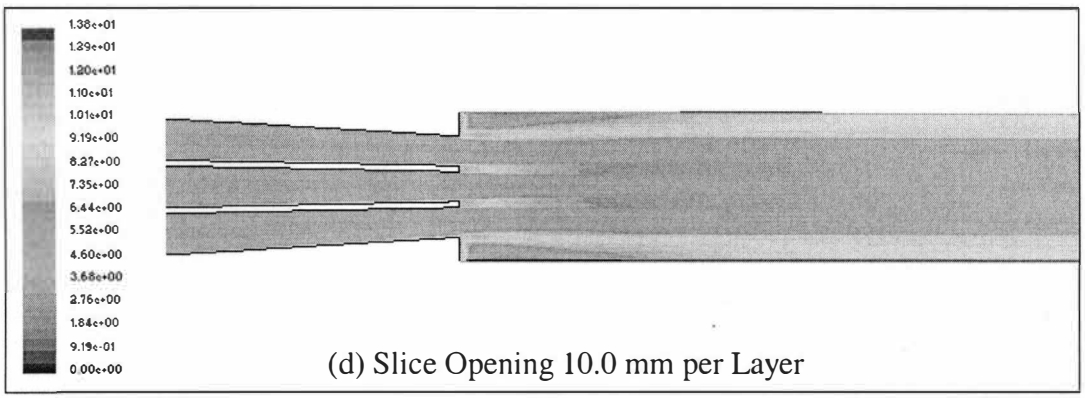

(d) Slice Opening 10.0 mm per Layer

Figure 33. Energy Dissipation (m^2/s^3) Contour of Slice Opening Case in Logarithmic Scale. (Continued)
(d) Total Slice Opening 34.0 mm. (10 mm per layer).

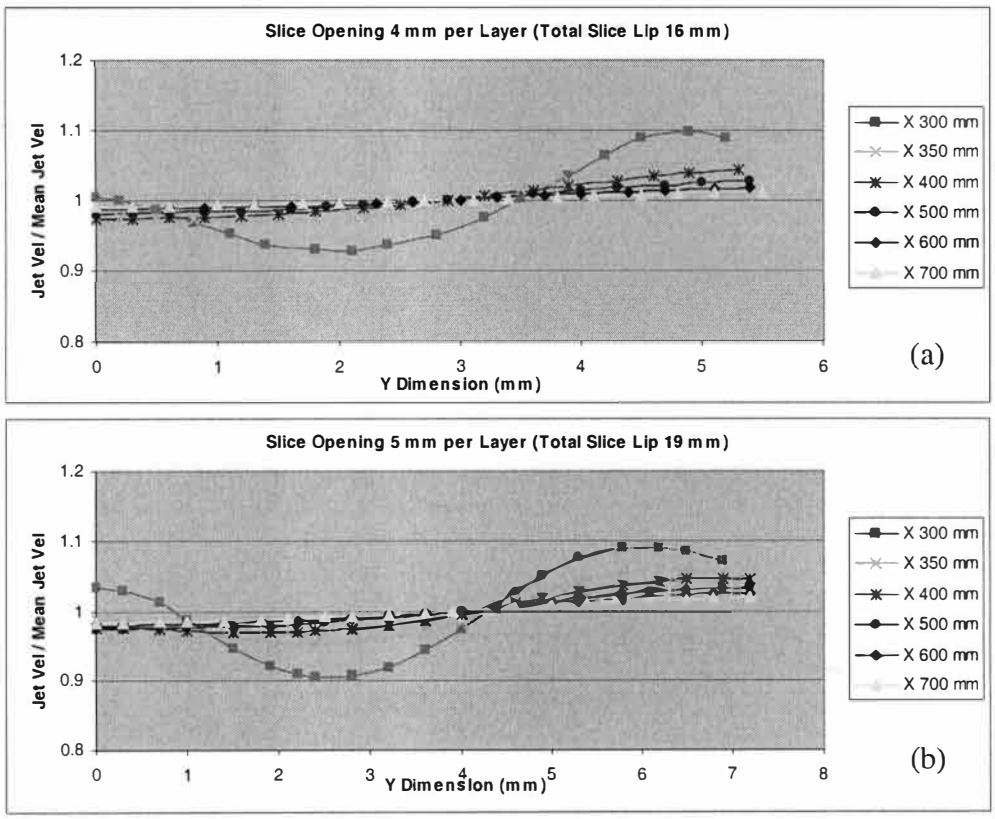

Figure 34. Relative Velocity Profile of Slice Opening Case.
(a) Total Slice Opening 16.0 mm. (4 mm per layer).
(b) Total Slice Opening 19.0 mm. (5 mm per layer).

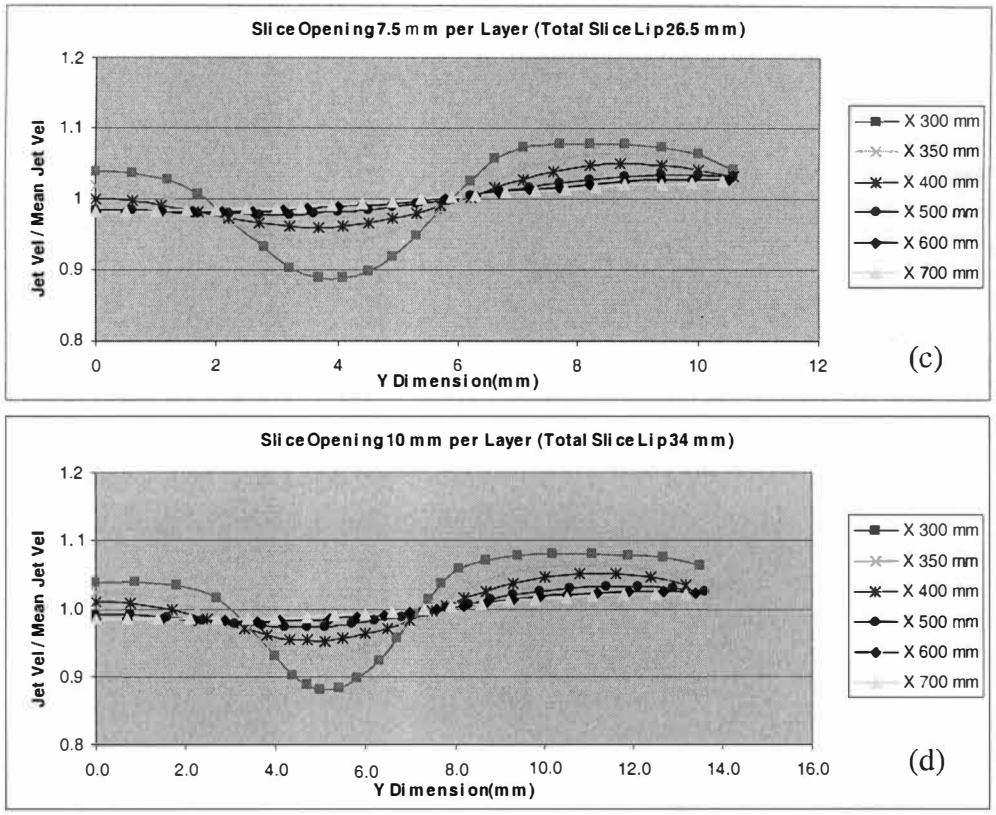

Figure 34. Relative Velocity Profile of Slice Opening Case. (Continued)
(c) Total Slice Opening 26.5 mm. (7.5 mm per layer).
(d) Total Slice Opening 34.0 mm. (10 mm per layer).

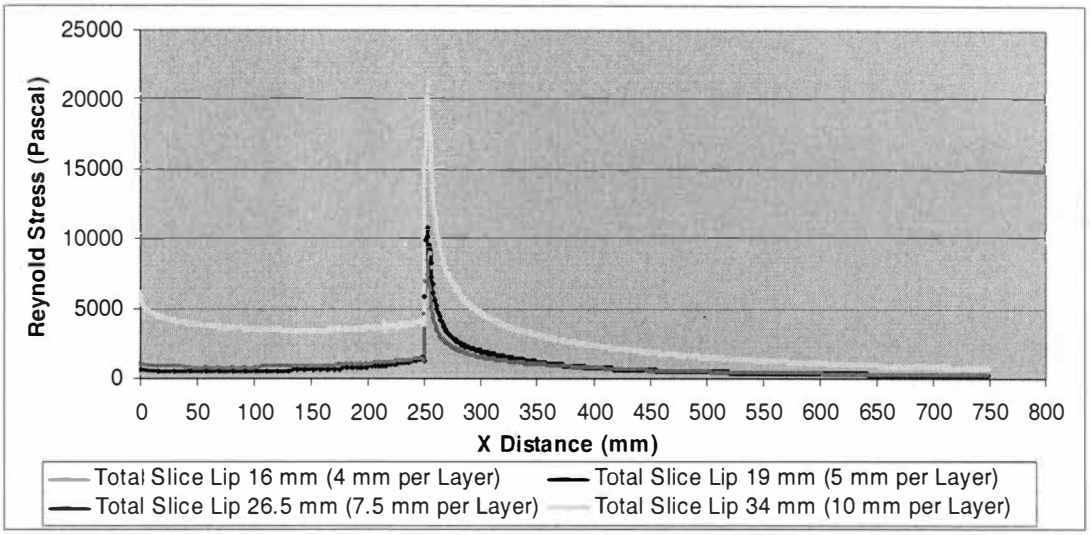

Figure 35. Reynolds Stress (Pascal) of Slice Opening Case.

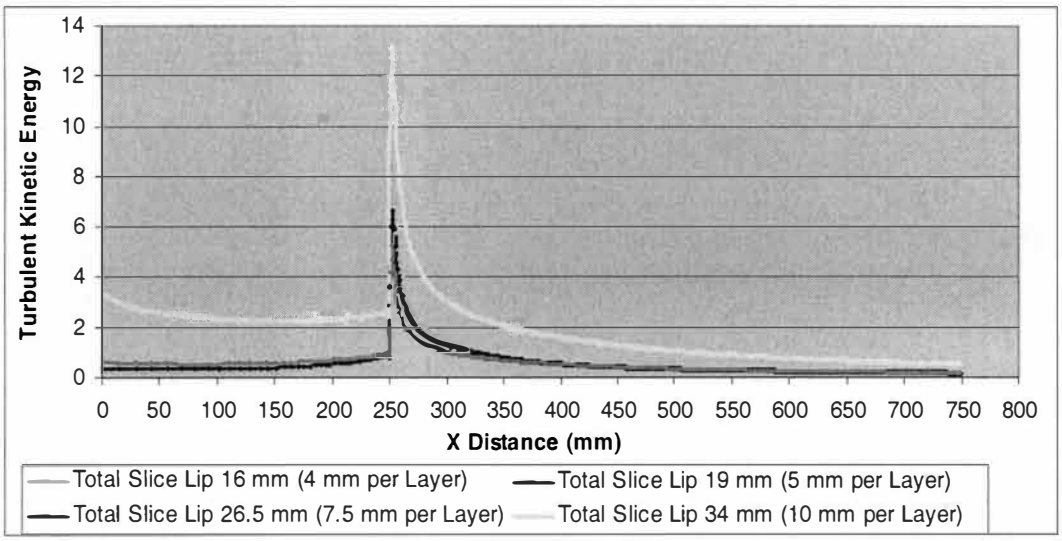

Figure 36. Turbulent Kinetic Energy (m^2/s^2) of Slice Opening Case.

It is clearly shown in Figure 37 that the wider slice opening produces larger macro scale of turbulence as the result in more layer mixing than narrower slice opening. However, the simulation result shows that the layer mixing is not much different if the free jet is less than 100 mm. Therefore, the narrow slice opening is

preferred to reduce the layer mixing and produce more uniform jet velocity profile. This conclusion is similar to the experiment by Lloyd and Norman [13].

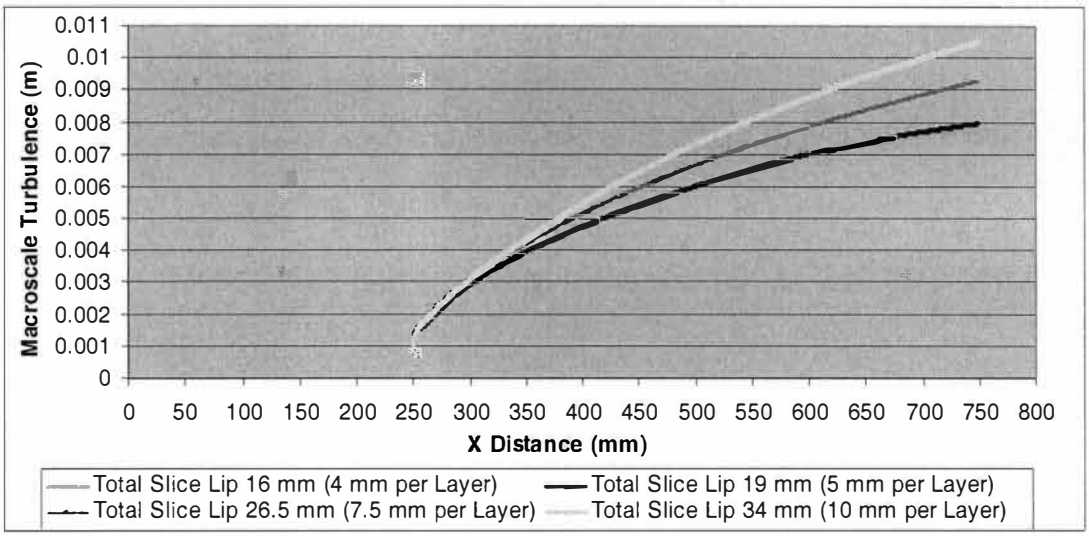

Figure 37. Macro Scale of Turbulence (m) of Slice Opening Case.

Three-dimensional Simulation of Stratified Headbox

A three-dimensional simulation is carried out to investigate the layer mixing in the free jet on the Cross-machine Direction (CD). The 3-D geometry of the head box and free jet is shown in Figure 38. Due to the symmetry assumption, only a half of the headbox and free jet is shown in Figure 38. The water fluid in the free jet is surrounded by the air with 10 mm thickness as shown in Figure 39.

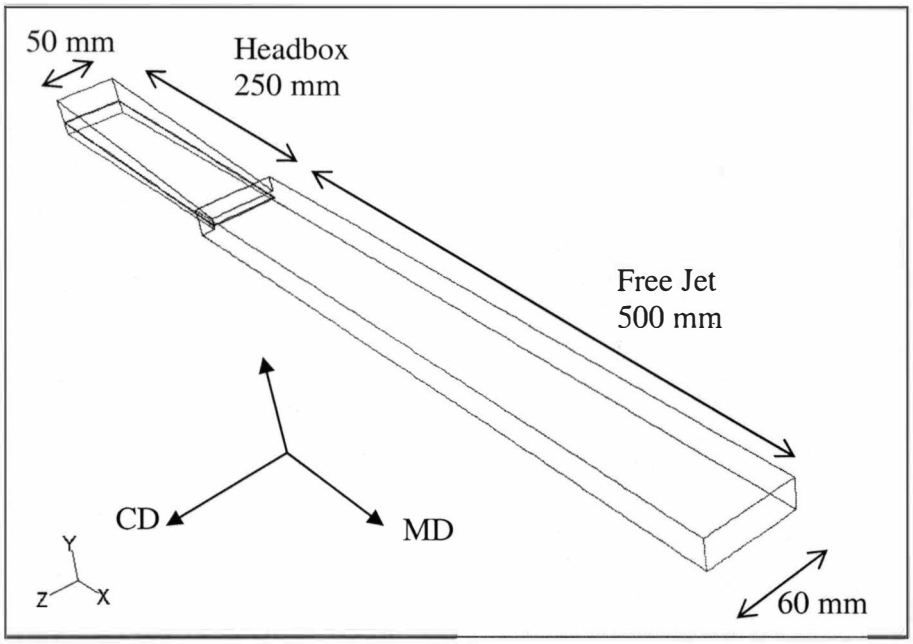

Figure 38. 3D Geometry of Headbox and Free Jet in 3D Case.

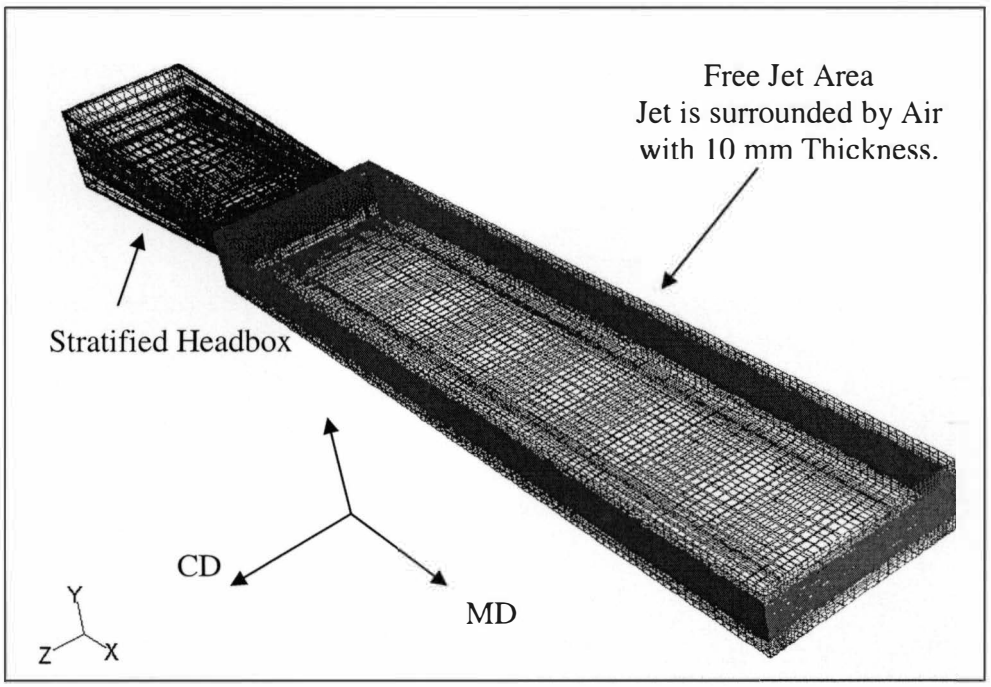

Figure 39. Headbox Model of 3D Case.

Importantly, the air entrainment is found in the free jet of the headbox. Figure 40 shows the results of volume fraction of water along the cross machine direction at the wake area just behind the vane. In this figure, the X-axis is in the cross-machine direction. The center in the cross-machine direction is located at 0.0 m and the sidewall is located at 0.05 m. The figure shows that the water fraction was decreased from 1 (water) at the center of the cross-machine direction to 0 (air) at the edge of headbox. A better visualization of air entrainment in terms of the fluid density contour (kg/m3) in the plane between the top layer and center layer is shown in figure 41.

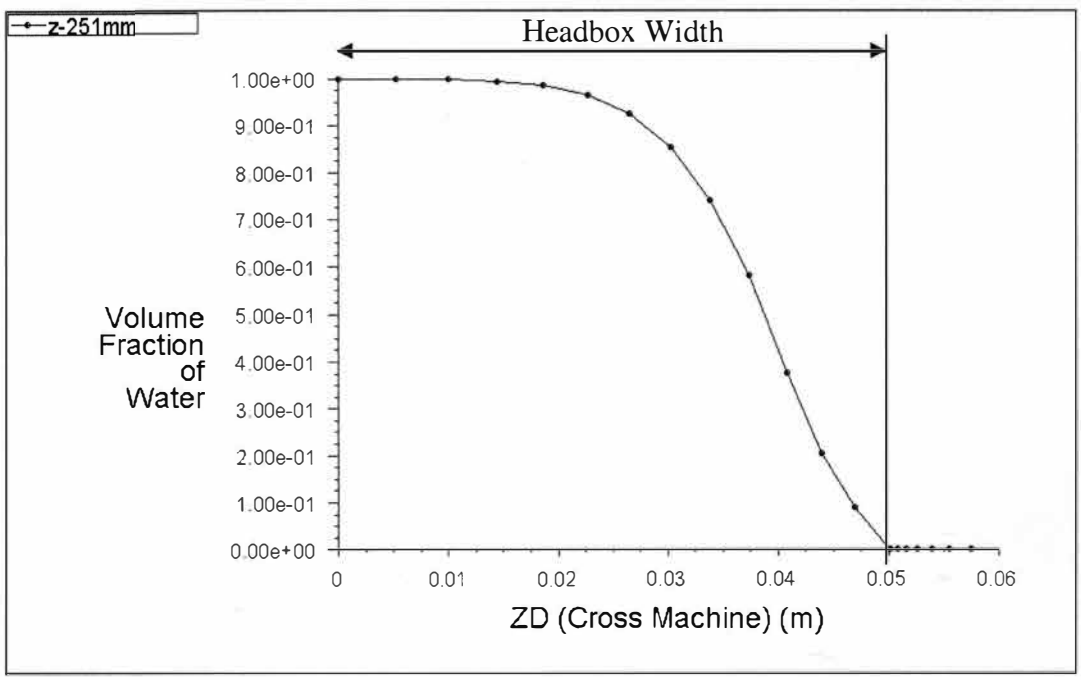

Figure 40. Plot of Volume Fraction of Water at The Wake Area Behind The Vane.

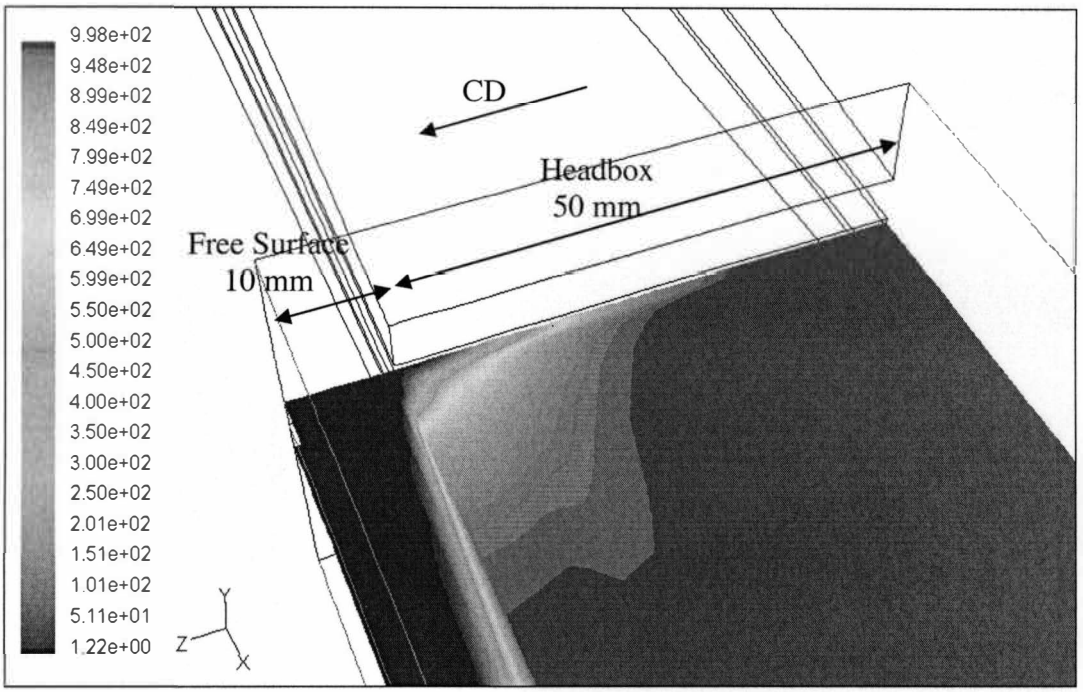

Figure 41. Density Contour (kg/m^3) on CD direction at the Plane between the Top Layer and Center Layer.

It is obvious that the air enters the free jet from the free surface area behind the vane around the edge of the headbox (see figure 41). The air enters 40 mm away from the jet edge. Air mixing with water may cause poor formation at the edge of the paper. Therefore, special attention should be paid on prevention of air entrainment around wake area behind the vane.

CHAPTER VI

CONCLUSION

A two-phase model, volume of fluid, is used to simulate the velocity profile, Reynolds stress, turbulent kinetic energy, macro scale of turbulences in the headbox and free jet. Surface tension is included in this model. The results show that it is possible to use the macro scale of turbulence, as the indicator of the layer mixing in the simulations of the free jet of stratified headbox, to optimize the vane length, free jet length, headbox angle, etc. It is found that the length of vane and free jet plays an important role on the layer mixing. The longer vane and the short free jet should be used to produce the fine scale of turbulence that leads to less layer mixing. In addition, to reduce the effect of the wake behind the vane on layer mixing, the angle of headbox has to be optimized and the thin vane should be used. In conclusion, it is expected that the vane and free jet lengths are the keys of layer mixing in a stratified headbox. It is better for both vane and free jet lengths to be adjustable during operation.

REFERENCES

1. Ewald, J. L., "Forming layered products allows best use of different furnishes", Pulp and Paper, Vol. 55 (April): 137-140 (1981)

2. Harwood, J.W., "Stratification of paper grades", TAPPI Journal, Vol.73 No.5: 115-122 (1990)

3. Page, R.E. and Hergert, R.E., "Enhancement of paper properties and fibre economics through web stratification", Appita Journal, Vol. 42 No.1: 33-41 (1989)

4. Parsheh, M. and Dahlkild, A.A., "Numerical modeling of mixing in stratified headbox jet", Engineering & Papermakers: Forming Bonds for Better Papermaking Conference, TAPPI (1997), pp. 1159-1174

5. Parker J.D., "The sheet forming process", TAPPI STAP, No. 9: 104 (1972)

6. Kerekes, R.J., "Pulp flocculation in decaying turbulence: a literature review", Journal of Pulp and Paper Science, Vol. 9: 86-91 (1983)

7. Kaarlo, N., "Paper Physics", Book 16 – Papermaking Science and Technology, Finnish Paper Engineers' Association and TAPPI (1998)

8. Ken L. Patrick, "Paper machine developments open door to higher quality, production efficiency", PPI Magazine, Vol. 72(6): 65-73 (1998)

9. Jatetana, K. and Dewei, Q., "3D Simulation of layer mixing in a three-layer stratified forming headbox", 2004 Paper Summit & Spring Technical Conference, TAPPI (2004)

10. Lloyd, M.D. and Norman, B., "Layer mixing during three layer stratified forming: The role of vane length and mix-wire speed difference ", TAPPI Proceeding, Engineering Conference, TAPPI (1996), pp. 193-208

11. Li, A.C., Neill, E.B. and Rogers, T.D., "Fundamental studies of mixing in a 3-layer stratified headbox jet", Journal of Pulp and Paper Science: Vol. 27 No.9: 306-309 (2001)

12. Li, A.C., Rogers, T.D., and Shands, J.A.,"Mixing intensity analysis of a two-layer stratified headbox jet", TAPPI JOURNAL Vol. 83 No.12: 59 (2000)

13. Lloyd, M.D. and Norman, B., "Effect of headbox slice geometry during the stratified forming of woodfree paper", Nordic Pulp & Paper Research Journal, Vol. 14 No. 4: 252-259 (1997)

14. Lloyd, M.D. and Norman, B., "Use of stepped vanes to alter headbox turbulence levels during stratified forming of woodfree paper", Appita Journal Vol.52 No.2: 98-104 (1999)

15. Farrington, T. E., Jr., "Numerical investigation of three tissue-machine headboxes", AlChE Forest Products Symposium Proceedings (Los Angeles), Nov 17-21 (1991), pp.177-188

16. Aidun, C.K. and Kovacs, A., "Hydrodynamics of the forming section: the origin of nonuniform fiber orientation", TAPPI Journal, Vol.78 No.11: 97-106 (1995)

17. Fluent Incorporated, "Fluent 5: User's Guide Volume 2", Fluent Incorporated, NH (1998).

18. B. Cardow, B. Mohammadi, and O. Pironneau, "A few tools for turbulence models in Navier-Stokes equations", Incompressible Computational Fluid Dynamics, Cambridge University Press (1993)

19. Fluent Incorporated, "Fluent 5: User's Guide Volume 3", Fluent Incorporated, NH (1998).

20. http://met4159-01.fa04.fsu.edu/Lecture4/lecture4.html

21. http://www.flow3d.com/Cfd-101/freesmod.htm

22. Fluent Incorporated, "Fluent 5: User's Guide Volume 1", Fluent Incorporated, NH (1998).

23. http://www.flow3d.com/Cfd-101/turb.htm